Archaeological Prospection

Joint interpretation of electrical and seismic data aimed at modeling the foundation soils of the Maredolce monumental complex in Palermo (Italy)

Journal:	*Archaeological Prospection*
Manuscript ID	ARP-20-0026.R1
Wiley - Manuscript type:	Special Issue Article
Date Submitted by the Author:	19-Sep-2020
Complete List of Authors:	Cafiso, Fabio; University of Palermo, Scienze della Terra e del Mare - DiSTeM Canzoneri, Alessandro; University of Palermo, Scienze della Terra e del Mare - DiSTeM CAPIZZI, PATRIZIA; University of Palermo, Scienze della Terra e del Mare - DiSTeM Carollo, Alessandra; University of Palermo, Scienze della Terra e del Mare - DiSTeM Martorana, Raffaele; University of Palermo, Scienze della Terra e del Mare - DiSTeM Romano, Filippo; University of Palermo, Scienze della Terra e del Mare - DiSTeM
Keywords:	Maredolce, Electrical Resistivity Tomography, Induced Polarization, Seismic Refraction, HVSR, geotechnical model

Joint interpretation of electrical and seismic data aimed at modeling the foundation soils of the Maredolce monumental complex in Palermo (Italy)

Fabio Cafiso, Alessandro Canzoneri, Patrizia Capizzi, Alessandra Carollo, Raffaele Martorana, Filippo Romano

Department of Earth and Sea Sciences, University of Palermo, Italy

Abstract

The monumental complex of Maredolce (Palermo) includes an Arab-Norman castle that stands on the banks of an artificial lake carved out of the calcarenitic rock that rests on impermeable clays. The lake was originally filled with water thanks to the channeling of a spring. Over time, the lowering of the water table and the high hydraulic permeability of the calcarenites have caused the lake to dry up. A project to renovate the monumental complex has recently been launched. It also provides the study of a possible restoration of the original conditions of the lake. To this end, a multidisciplinary geophysical study was carried out to investigate the geotechnical conditions of permeability of the land outcropping and provides valid technical solutions for waterproofing the bottom of the lake. For this purpose, a joint interpretation was performed using data acquired with different geophysical techniques, such as seismic refraction tomography, electrical resistivity and induced polarization tomography, multi-channel analysis of surface waves and Horizontal to Vertical Spectral Ratio of environmental vibration recording. Joint interpretation, supported by cluster analysis techniques, allowed the reconstruction of the geophysical and geotechnical model of the subsoil of the ancient lake, helpful to suggest appropriate techniques for waterproofing the bottom of the lake.

Introduction

The Monumental Complex of Maredolce (fig. 1) is one of the Arab-Norman monuments of Palermo, declared "World Heritage". The complex includes a building, born as an Arab fortification, and 25 hectares of garden, still cultivated with citrus groves.

The cultivated area of the garden is located on a plateau a couple of meters above a depression that was once an artificial lake fed by a spring: the “Grande Favara” (from the Arabic "al-fawwāra", the spring). The lake once surrounded the building on three sides, creating an environment of incredible beauty (Trapani, 2014). Unfortunately, after the abandonment of the castle, the spring water was brought elsewhere and the lake dried up.

The restoration project involves the reconstitution of the artificial lake, called Maredolce, and the recovery of the original morphology of the places. Furthermore, the entire monumental complex, the Arab-Norman building and the surrounding citrus grove will be recovered.

The reconstruction of the geological, hydrogeological and geotechnical model of the whole area is necessary for the realization of the restoration project.

In fact, in the outcrop there is the Pleistocene sandy-calcarenitic complex of the Palermo plain, characterized by a high permeability for cracking and porosity.

The geotechnical modeling specifically concerned the permeability properties of the soils present in the area under study, as the main objective of this study is to identify the problems of hydraulic sealing of the artificial lake that is to be reconstituted and any techniques to refer to achieve that goal. Based on the results obtained, it is necessary to provide for the use of waterproofing techniques at the bottom of the artificial lake, according to the principle of optimizing the hydraulic seal and the naturalistic requalification of the site starting from the reconstitution of an aquatic environment suitable for the development of flora and fauna.

With this in mind, a multidisciplinary study has been launched whose first results indicate bentonite geocomposites as the solution that at the same time optimizes the hydraulic aspects and the landscape-environmental requalification of the Monumental Complex of Maredolce.

Several geophysical investigations were carried out on the site to identify the waterproof levels in the subsoil and the piezometric surface. In particular, electrical and active and passive seismic methods were performed, the joint interpretation of which, constrained by the geological survey and drilling data available in the area (Todaro, 2016), allowed to carry out a 3D lithological and geotechnical modeling of the subsoil of the monumental complex.

Historical features

At the gates of Palermo, on the eastern outskirts of the city, in the heart of the Brancaccio-Ciaculli district, stands the monumental complex of the Favara-Maredolce (from the arabic *al-fawwāra*, "the spring"). Originally, it extended along this sector of the Conca d'Oro around an area between the slopes of Pizzo Sferrovecchio, the northern offshoot of Monte Grifone, and the coast.
The site is part of the monuments of the Arab-Norman Palermo circuit and was built by order of the Norman King Roger II of Altavilla in the 12th century, becoming one of the so-called "*solatii regii*" (king's comforts). Its strategic importance, combined with the amenity of the place, explains the choice of this site for the creation of one of the parks preferred by Roger II, the "*Parcus Vetus*" ("Old Park"), the oldest of the Norman parks in Palermo, as well as the oldest suburban park in Europe.

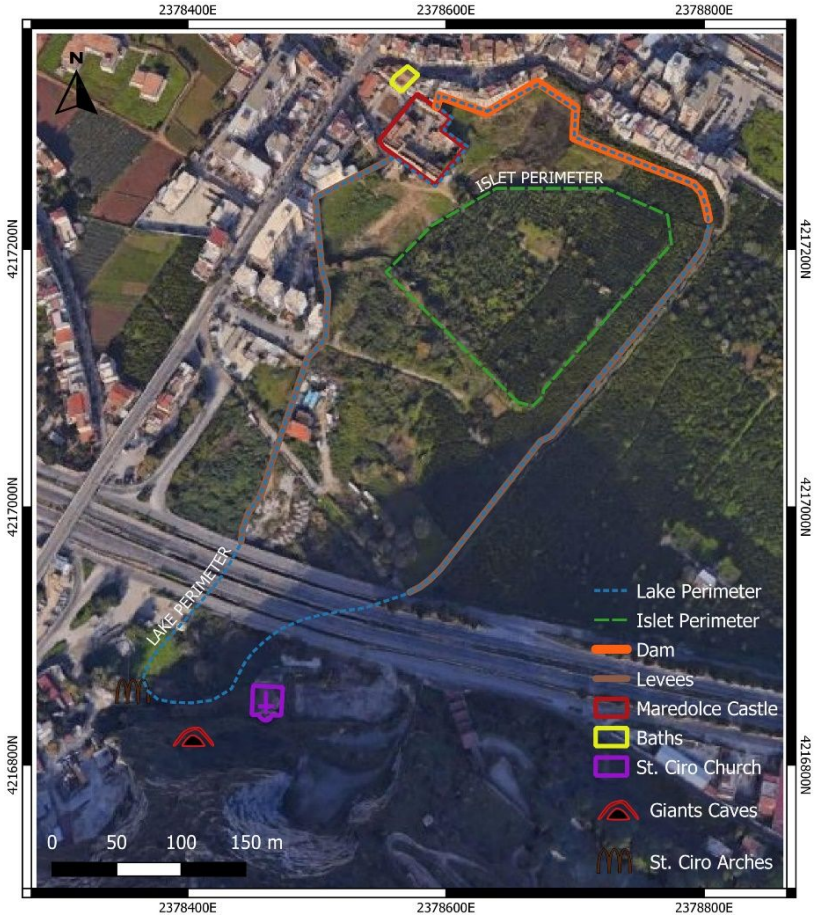

FIGURE 1: *Elements of the Favara-Maredolce monumental complex.*

Built according to the type of *agdal* gardens, typical of the Arab-Persian territories, the site today presents a vast depression of the ground, on which once insisted a large artificial lake rich in fish (*al-buhayra*), enclosed downstream by a masonry dam and fed by the abundant waters of the Favara spring (*al-fawwāra*), which lapped the ancient palace on three sides (fig. 1). The fishing lake was so wide thus being called "*Maredolce*" (freshwater sea), at the centre of which emerged an irregularly shaped islet reachable by boat. The whole complex, once surrounded by beautiful

gardens full of palm trees, orchards, citrus groves and various species of exotic animals, represented a rare historical-environmental testimony that documented the Koranic culture of the "*Paradise Gardens*" (*Jannat al-ard*, or "*Genoardo*") in the West. The perfect balance between greenery, water and architecture achieved a perfect aesthetic harmony in these sites which they were able to enjoy kings and emirs (Barbera, Boschiero, & Latini, 2015).

The evidence of a first settlement in the area dates back to the Roman-Republican age (III-II century BC) and probably refers to a rural complex built in the middle of a very favorable natural context for the presence of abundant quantities of water and flat land suitable for agro-pastoral kind of activities.

There is no archaeological data after this first phase, until the 10th century, when with the Arab domination begins the real history of the site. Thus, on the remains of the Hellenistic settlement, at the end of the 10th century, a palace was built consisting of large calcarenite blocks, according to the canons of the *qasr* (from the Latin "*castrum*"), and known as *Qaṣr Jaʿfar* (Giafar Palace), a small fortification built by order of the Emir Kalbi *Jaʿfar al-Kalbī II* (997- 1019). This building phase is associated with a surrounding area, which was crossed by a natural impluvium, where the abundant spring waters flowed, and by a series of irrigation channels which suggest an agricultural use of the fertile land (Amari, 1939).

But it was only with the conquest of the island in 1091 by the Normans that the monumental complex reached its maximum glory: on the base of the pre-existing Arab one, Roger II had built the new palace, inside which various rooms were built around a rectangular courtyard bordered by an arcade. Three entrances characterize the main facade of the palace: the first leads to the central inner courtyard, the second to the Byzantine chapel of Saints James and Philip, consisting of a single nave and a presbytery with its hemispherical dome, and the third to the royal hall with its pleated vault and the adjoining room dedicated to the Koranic cult with the presence of three *muqarnas* on the southern wall (fig. 2). A room known as the "*Imbarcadero Hall*" leads outside where the fishing lake was built, in which the kings sailed on boats. The spring, now extinct, was protected by a building located at the foot of Pizzo Sferrovecchio and known as the "*Saint Ciro Arches*": it is composed of three rooms covered by barrel vaults with an ogival section, whose function was certainly that of intake, water regulation and spring protection (Todaro, 2015).

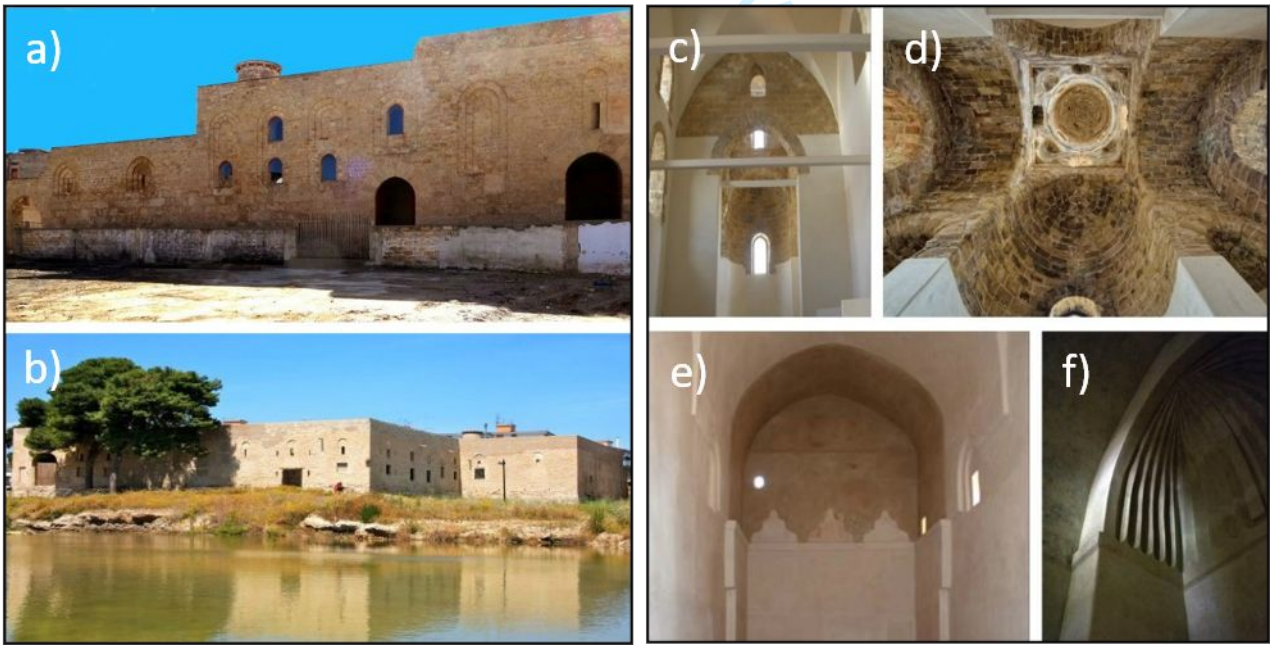

FIGURE 2: *The Castle of Maredolce: a) the main facade with the three entrances; b) the palace seen from the lake; c) the chapel of Saints James and Philip; d) the hemispherical dome of the chapel; e) the muqarnas and f) the pleated vault of royal hall.*

Celebrated by the poets and travelers of the time, after the Norman and Swabian age, the monumental complex underwent profound transformations, both in form and function, assuming a configuration that refers to an almost exclusively agricultural use during the following centuries. Fallen definitively in abandonment, the palace was used as a dwelling and divided into various units by different owners who made significant transformations. Today the monumental complex finally belongs to the state property of the Sicilian Region, which has entrusted its recovery and restoration to the Superintendence of Cultural and Environmental Heritage of Palermo. The recovery project of the monumental complex of the Favara-Maredolce received in 2015 the prestigious "*Carlo Scarpa International Award for the Garden*", XXVI edition, promoted by the Benetton Studies Research Foundation.

Geological setting

The geological structure of the Favara-Maredolce monumental complex is part of the more general context of the formation of the Palermo Plain: the latter, in fact, consists of a large morphostructural depression characterized by a large calcarenite marine terrace and is connected to the Pleistocene tectonic phase (Abate, Catalano, & Renda, 1978) that dismembered the overlapping flaky structure of the Palermo Mountains formed during the Miocene, contributing to the collapse of its northernmost areas through high angle normal faults and syndepositional listric faults with considerable throw, which have displaced in various blocks the Mesozoic substrate and the related coverings of the Oligo-Miocene clays of the Numidian Flysch (Contino, Giammarinaro, Vallone, Varsalona, & Zuccarello, 2006).

The progressive increase of the accommodation space in the tectonic depressions at the hanging wall of the normal faults and the repeated oscillations of the sea level during the Pleistocene allowed the deposition of marine deposits in sub-horizontal layers (Agate, et al. 2017): the latter, in fact, seal the faults with throws of hundreds of meters and rest in unconformity on the clays of the Numidian Flysch or directly on the Mesozoic carbonates surrounding the Palermo Plain.

The Favara-Maredolce site is characterized by a strong contrast of geomorphological features that compare the calcarenite plain of Brancaccio, the slender foothills area of Saint Ciro and the overhanging steep slopes of Pizzo Sferrovecchio. The current morphology of the area is the result of tectonic-sedimentary processes and of an intense selective erosion activity that has mainly worked on two types of outcropping rocks: from the calcarenites in horizontal layers of the flat Pleistocene terrace, to the gray carious Mesozoic dolomites with a massive structure and intensely fractured and karstified of Pizzo Sferrovecchio.

The site is limited by a system of direct faults with considerable throw responsible for the dislocation in various blocks of the Mesozoic dolomitic substrate of Pizzo Sferrovecchio and the terrigenous coverings of the clays of the Numidian Flysch which are hydraulically configured as an underground barrier that favours the transfer of water into the calcarenite plain, with the formation of a series of springs in the foothills area. Since ancient times, in fact, the remarkable underground water productivity of the Favara-Maredolce site was due to the abundant water that flowed from the numerous fissures of the dolomitic rock (water springs) of the nearby Favara spring on the slopes of Pizzo Sferrovecchio, ending up in the depressed area of the calcarenite plain in front of it, where the seasonal rising waters stagnated. In fact, the site is characterized by the presence of two aquifers: a superficial one, made up of Pleistocene calcarenites, permeable by porosity and hydraulically buffered by the underlying gray-blue clays that are not very permeable, and another deep one, made up of the highly permeable dolomitic soils of Monte Grifone due to fracturing and karst (Todaro, 2016).

In spite of all this, the substantial evolution of the Maredolce site was strongly conditioned by the anthropic transformations that it has undergone since the Middle Age, with the construction of an artificial basin (Maredolce lake) attributed to King Roger II, who wanted to exploit the nearby Favara spring waters to create his place of amusement, capturing and regulating them through the construction known as the "Saint Ciro Arches", located on the slopes of Pizzo Sferrovecchio.

As part of the multidisciplinary project of the Superintendence for Cultural and Environmental Heritage of Palermo aimed at the recovery of the monumental complex of the Favara-Maredolce, Todaro (2015) has come to the realization of a 2D geological model of the lake basin, through a preliminary stratigraphic study. From the information contained in the "CityGIS" geological database of the city of Palermo (Giammarinaro, Canzoneri, Vallone, & Zuccarello, 2003; Giammarinaro, Maiorana, & Vallone, 2003), a continuous core drilling survey, carried out in 1999 by Todaro and named "0433", has been extracted, which revealed three different lithological units, one of which is continental, consisting of lake, peat and colluvial deposits sedimented by the spring waters of the Favara, and two of marine environment, deposited in a Pleistocene transgressive-regressive sedimentary cycle, with calcarenites on the top and clayey silt at the bottom.

The core drillings located near the monumental complex (see e.g. core drilling "1198" in fig. 3) confirm the stratigraphic succession, apart from the lake sediments.

The lithostratigraphic series of the soils present in Maredolce, obtained from the survey up to a depth of 20 m, is made up, from the oldest to the most recent, of the following lithotypes (Catalano, Avellone, Basilone, Contino, & Agate, 2013):

- ***Ficarazzi Clays***. Fine silty sands, with intercalations of sandy clays and grey-blue coloured silts, little thickened and compressible. Their thickness is 16.3 m. *Pleistocene (Sicilian)*.
- ***Palermo Calcarenites***. Yellowish calcarenites, tender, with a discontinuous stratum-nodular structure and sands with nodules, in horizontal position, variously decemented due to the oscillation of the shallow water table. Their thickness is 2.40 m. The formation hosts a water table whose piezometric level, variable with the seasons, was measured in April 1999 at a depth of 2.80 m from the ground floor. *Pleistocene (Calabrian)*.
- ***Lake deposits***. They represent the "past memory" of the basin and are made up of alternating laminar layers varying in thickness, composition and texture, according to seasonal variations and the activity and flow of the Favara spring ("varve", if referred to one year). The series is closed by the "*residual red soils*" that constitute the most superficial pedogenized blanket on the islet. *Holocene*.

Geophysical measurements

The purpose of the geophysical studies carried out on the site is to investigate and geometrically characterize the levels belonging to the lithologies which are considered impermeable within the succession present in the subsoil. The combined and integrated use of different tomographic methods, such as electrical resistivity, induced polarization and refraction seismics, has often proved useful in environmental or archaeological applications (Cardarelli & Di Filippo, 2004; De Domenico, Giannino, Leucci, & Bottari, 2006; Deiana, Leucci, & Martorana, 2018). Following a similar approach, the integrated application of electrical resistivity tomography, induced polarization and seismic refraction tomography was considered, as well as surface waves methods and seismic microtremor measurements (fig. 3).

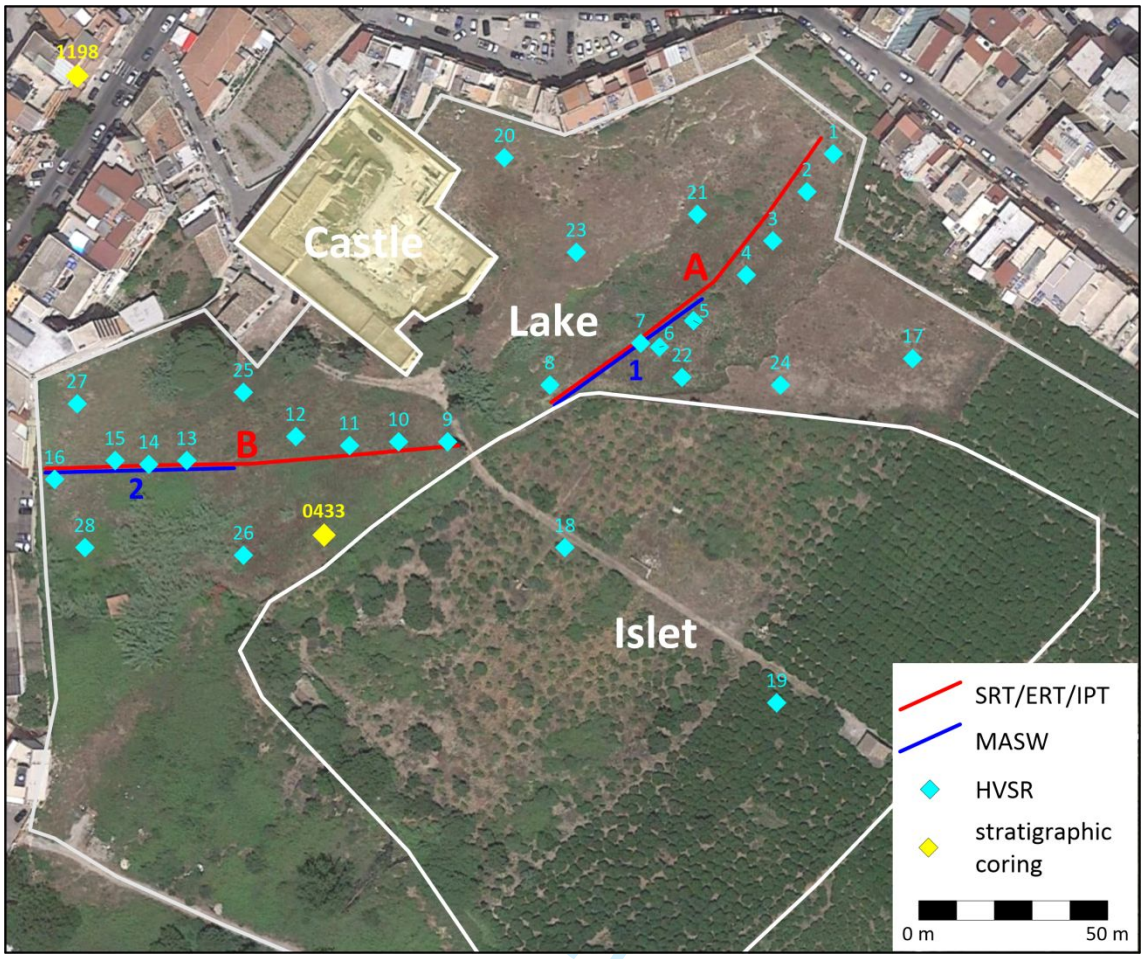

FIGURE 3: *Aerial photo of the monumental complex of Maredolce, with the locations of the geophysical surveys carried out and the core drillings.*

Seismic Refraction Tomography

The Seismic Refraction Tomography (SRT) is a seismic investigation method used to investigate the structure of the Earth based on the analysis of the propagation times of seismic waves. By observing the propagation of elastic waves, it studies the behavior of rocks by identifying the paths and speeds with which they propagate in the ground, in order to be able to reconstruct the geometry and nature of the subsoil based on the presence of elastic discontinuities. The main objective of seismic tomography is to detect the path of the seismic ray as well as the shortest travel time (time of first arrival of the seismic waves) that elapses between the source and the receiver. In general, the seismic tomography is a data inference technique that uses information contained in seismic records to constrain 2D or 3D models of the Earth's interior. It generally requires the solution of a large inverse problem to obtain a heterogeneous seismic model that is consistent with observations (Rawlinson, Pozgay, & Fishwick, 2010).

Two alignments have been considered for the seismic refraction tomographies (SRT), electrical resistivity tomographies (ERT) and Induced Polarization Tomography (IPT), 98 m long each (fig. 3). Line A is located in the depression to the east of the Castle, roughly oriented NE-SW, for a length of 98 meters, line B it is instead located in the depression to the south-west of the castle, with orientation approximately E-W, and the same length as the line A. In both lines electrodes and geophones have been placed in coincident positions and distance equal to two meters, in order to allow a joint interpretation of SRT, ERT and IPT, using cluster analysis techniques (Capizzi, Martorana, Carollo, & Vattano, 2017; Carollo, Capizzi, & Martorana, 2020).

For each seismic refraction tomography survey, 48 geophones were used, spaced 2 m, and 13 shot points were considered (fig. 4, a), disposed with intervals of 8 m between the geophones, in

order to ensure good lateral coverage, thus obtaining 624 seismograms. The MAE X610S high resolution digital seismograph was used to acquire seismic signals.

The data were processed and inverted with Rayfract® software (Intelligent Resource, Inc.) ver. 3.35. Rayfract® software processes a reliable imaging of the seismic velocity trend in the subsoil through a modeling of the propagation of seismic energy associated with the first arrivals.

A manual picking of each track was made to estimate the first arrival times of the P-waves (fig. 4, b); thus, the data obtained have been inverted using the Delta-tV method (Gibson, Odegard, & Sutton, 1979) which automatically generates an initial 1D model (Gebrande, & Miller, 1985; Rohdewald, 2011), to identify small characteristics and velocity inversions. Subsequently, it uses the WET (Wavepath Eikonal Traveltime) method (Schuster, & Quintus-Bosz, 1993), WET tomography models the multiple paths of the signal volume propagation that contribute to a first arrival.

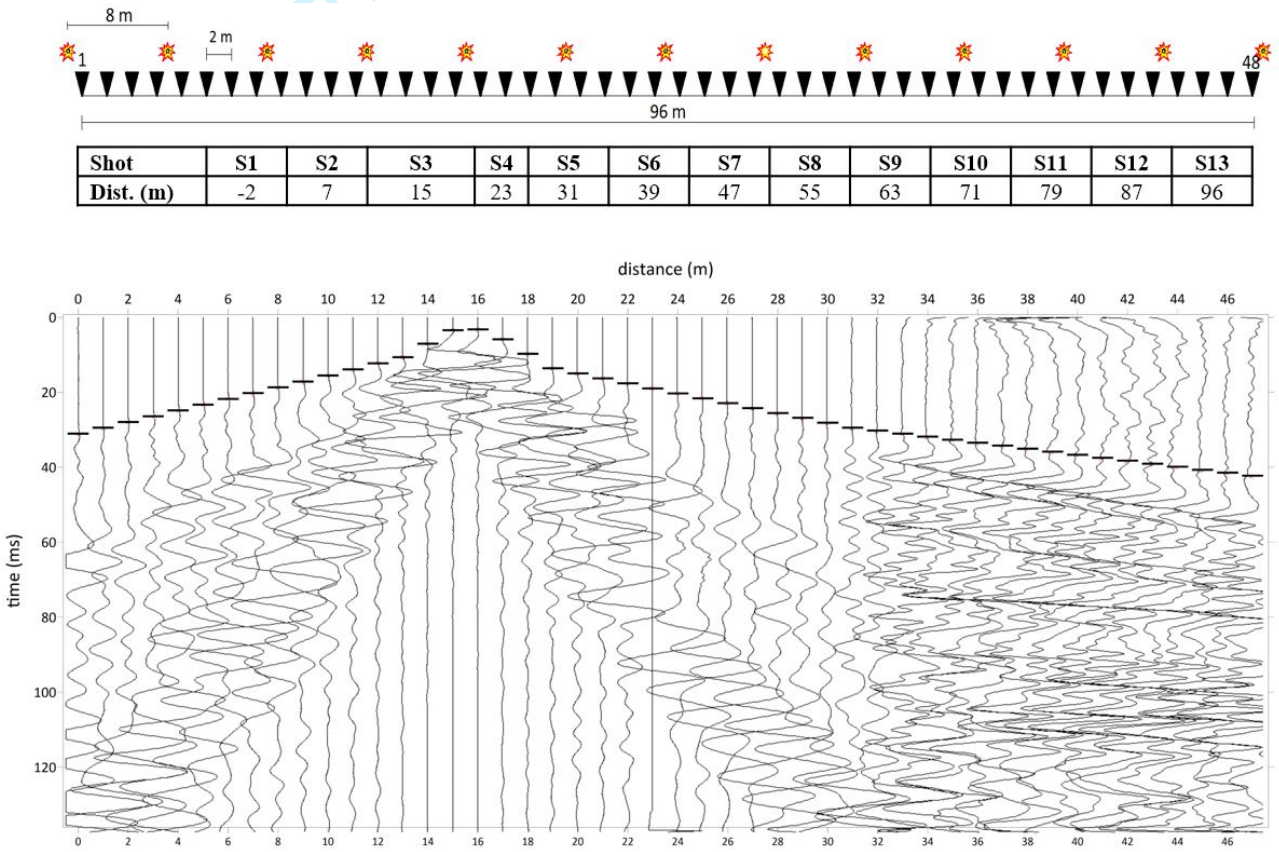

Shot	S1	S2	S3	S4	S5	S6	S7	S8	S9	S10	S11	S12	S13
Dist. (m)	-2	7	15	23	31	39	47	55	63	71	79	87	96

FIGURE 4: Surveying scheme of the Seismic Refraction Tomographies (top) and an example of seismograms related to the shot 5 of the SRTA (bottom), showing the picking of the first arrival times.

Figures 5 and 6 show the results of the data inversions. From the inversions two distribution maps are obtained, (i) of the propagation velocity of the P-waves with respect to the depth, and (ii) of the density of seismic rays with respect to the depth. The inversion obtained with respect to line A shows for the first meters of the subsoil, variable velocity between 800 m/s and 1200 m/s. It is noted that the velocity of seismic waves increases with depth, for the subsequent layers, reaching a velocity of about 2000 m/s (fig. 5, top).

From the seismic ray distribution map (fig. 5, bottom) the passage between the two described layers is evident, probably interpretable from a surface clayey soil, in contact with the underlying calcarenites. It is also evident a further stratigraphic limit below the calcarenites, where there is a decrease in the density of seismic rays and an increase in the velocity of seismic waves (velocity greater than 2000 m/s), probably corresponding to the Ficarazzi clays.

In addition, in the inversion obtained respect to line B, there is a progressive increase in seismic wave velocity with depth, from 800 m/s to 3500 m/s (fig. 6, top). The coverage of two lithologies is evident, probably due to the contact between the clay soil, which has a low density of seismic rays, and the underlying calcarenites, which show a high density of seismic rays (fig. 6, bottom). It is very probable that below the calcarenites there are the Ficarazzi clays, with velocity certainly superior than 2500 m/s.

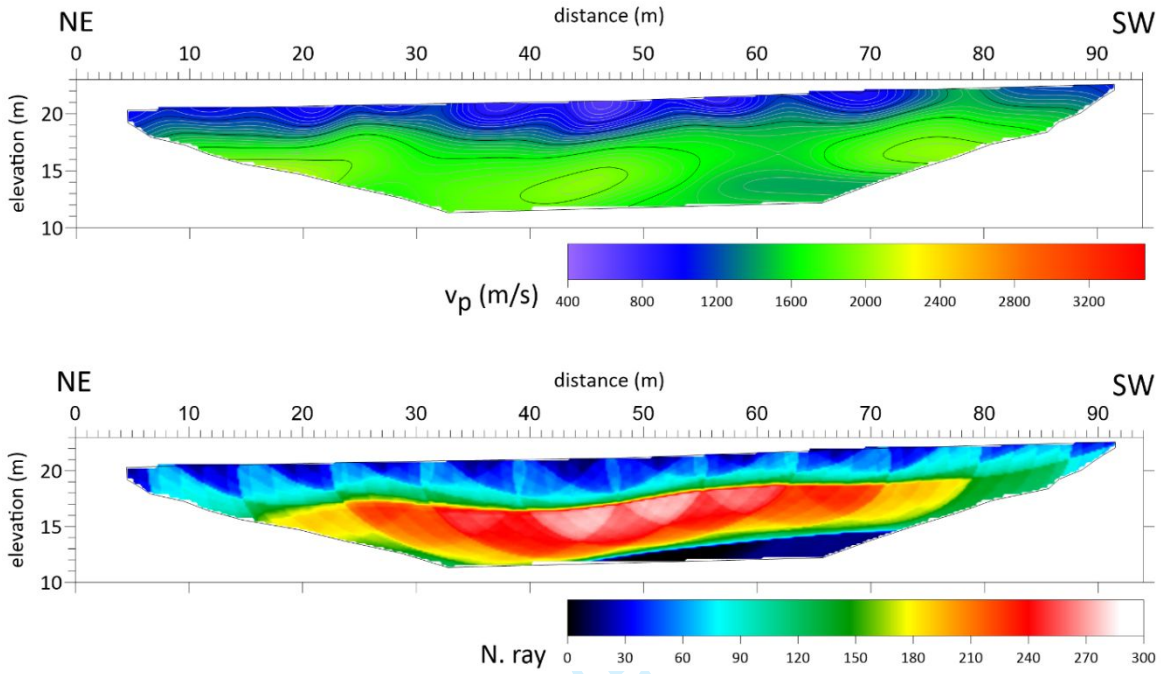

FIGURE 5: *Seismic Refraction Tomography line A: P-waves velocity (top) and raypath density (bottom).*

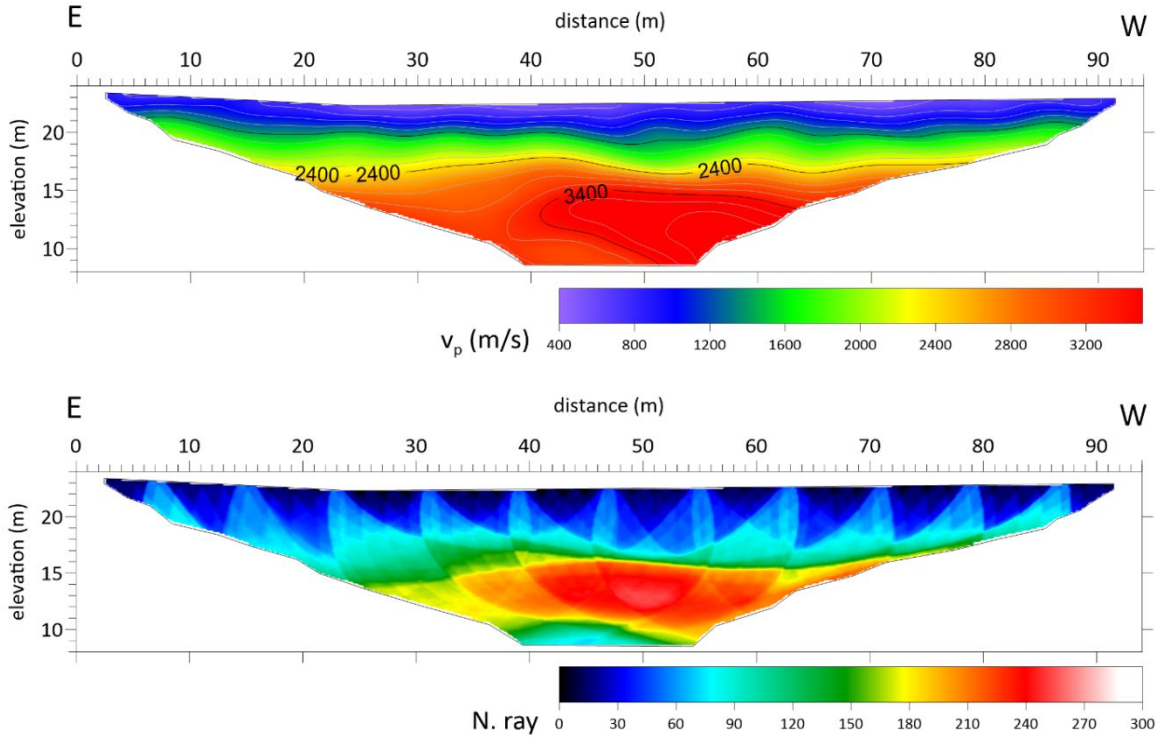

FIGURE 6: *Seismic Refraction Tomography line B: P-waves velocity (top) and raypath density (bottom).*

Electrical Resistivity and Induced Polarization Tomography

The resistivity method is one of the most commonly used geophysical exploration methods in archaeological exploration investigations (Griffiths, & Barker, 1994; Tsokas, Tsourlos, Vargemezis, & Novack, 2008) but also for hydrogeological applications (Koch, Wenninger, Uhlenbrook, & Bonell, 2009; Robert et al., 2011; Martorana, Lombardo, Messina, & Luzio, 2014). It estimates the electrical resistivity of the subsoil based on the relationship between electrical resistivity, current and potential, described by Ohm's law. Measurements are made by injecting an electrical current into the ground through two current electrodes and measuring the resulting voltage difference at two potential electrodes. In the last years, recent developments in field instrumentation and inversion algorithms have allowed to achieve significant improvements in 2D electrical resistivity tomography (Loke, Wilkinson, Chambers, Uhlemann, & Sorensen, 2015). The solution of the direct problem for 2D models can be based on the finite difference method (Dey, & Morrison, 1979; Pidlisecky, Haber, & Knight, 2007) or the finite element method (Coggon, 1971), discretizing the subsoil in a grid of cells to obtain an adequate representation of the trend of electrical resistivity (Loke, Acworth, & Dahlin, 2003). The inverse problem is non-linear and ill-posed and must be addressed by iteratively solving the forward problem and trying to minimize the misfit between the observed and predicted data.

Electrical resistivity contrasts can be indicative of lithological changes (Lapenna et al., 2003), rocks with different porosity or zones with different water content (e.g. Lehmann et al., 2013). However, the presence of clay sediments is also related to low electrical resistivity values due to the conduction mechanisms that take place on the negatively charged surface of the clay minerals (Revil, & Glover, 1998). Therefore, the quantitative interpretation of the ERT results can be challenging, considering the impossibility of discriminating if the variation in electrical resistivity is caused by the variability of porosity, water content or clay. In these cases, it may be useful for the interpretation to combine the ERT surveys with the Induced Polarization Tomography (IPT) (Gonzales Amaya, Dahlin, Barmen, & Rosberg, 2016; Chirindja, Dahlin, Juizo, & Steinbruch, 2017). This is an extension of the ERT technique, which provides information on the electrical conduction and capacitive properties (polarization) of the subsoil (Kemna et al., 2012). IPT can be useful for solving the distribution of electrical properties of the subsoil, which are strongly linked to clay and water content (Slater, Ntarlagiannis, & Wishart, 2006; Grandjean, Gourry, Sanchez, Bitri, & Garambois, 2011; Merritt et al., 2014; Okay et al., 2014).

ERT and IPT measures were simultaneously carried out (Griffiths, & Barker, 1994), using the MAE X612-EM+ resistivity-meter. This multielectrode instrumentation allows the simultaneous acquisition of all voltage measurements relating to a determined current dipole, so allowing, with an appropriate array sequence, a high surveying speed. The chosen array sequence is a particular dipole-dipole array sequence, which comprises 882 measurements. This is optimized for multi-channel instrumentation, considering the highest ratio between number of potential measurements and current dipoles used, so as to obtain the highest number of measurements in the shortest time possible, while ensuring a sufficiently regular distribution of points and, consequently, a high resolution and a great depth of investigation (Martorana, Capizzi, D'Alessandro, & Luzio, 2017). For this sequence, a maximum geometric factor of 1000 m was imposed, to limit the signal-to-noise ratio. This sequence allowed to reach a depth of about 14 m for both tomographies.

The acquired data were filtered by discarding those with current intensity lower than 10 mA and those which had a standard deviation for the apparent resistivity greater than 15%. In this way a reduced set of 640 data for ERT A and 840 measurements for ERT B has been chosen. The selected apparent resistivity measurements show values between 10 and 70 Ωm with an average of 25 Ωm for ERT A and between 18 and 125 Ωm with an average of 32 Ωm for ERT B.

Apparent resistivity and chargeability measures were inverted using the RES2DINV software (Loke, 2013). Inversion process was carried out considering a very fine mesh for the inverse model, of a quarter of electrode distance, considering the high number of measures processed. The damping factor was automatically optimized for each iteration. A joint inversion method was used for IP measures using an apparent IP cutoff value of 400 mV/V. For both tomographies, inversions stopped after 5 iterations, causing the misfit to drop to acceptable values, considering the high noise generated by high contact resistances to the electrodes and the large number of data used. ERT A and ERT B shows a RMS error of, respectively 15.5% and 6.5%, instead IPT A and IPT B shows a misfit of 41.2% and 38.1%. The relative sensitivity distribution is showed in fig. 7. On the basis of the decrease in sensitivity, we decided to consider the maximum investigation depth that for which the value was greater than 0.2, thus obtaining a depth of 10 m for ERT A and 15 m for ERT B. The difference is caused by the greater noise from ERT A data which forced to discard measurements with a larger geometric factor.

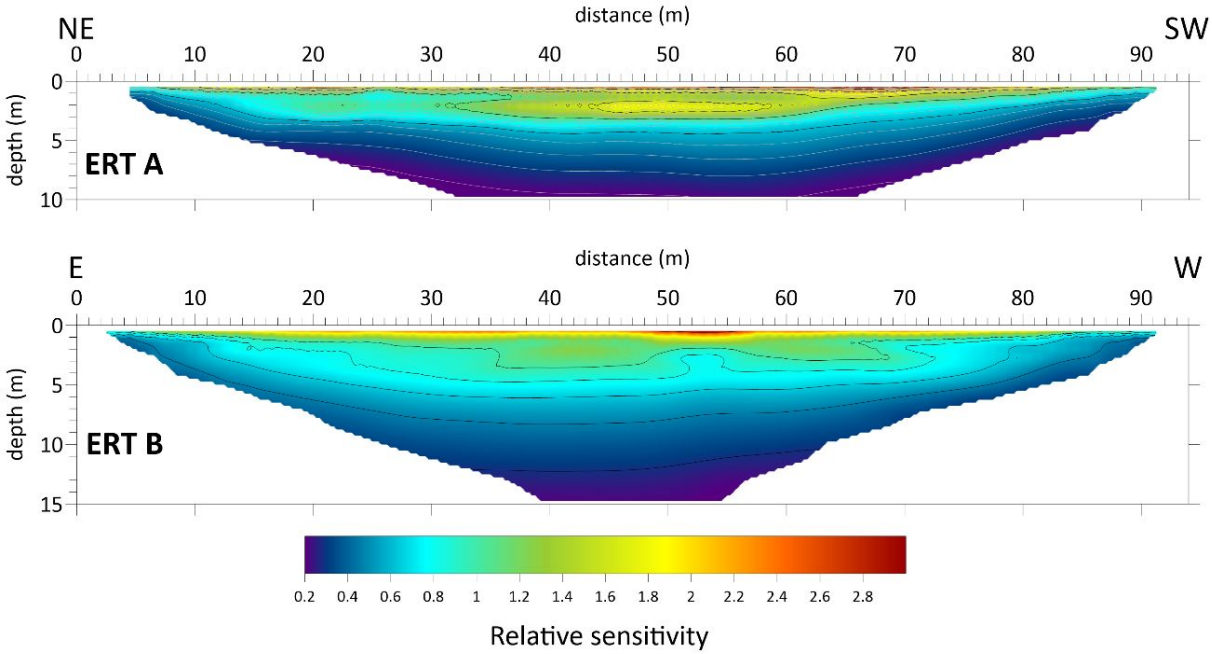

FIGURE 7: *Pattern of the relative sensitivity of the electrical resistivity tomographies carried out in the Maredolce Lake.*

The ERT results (fig. 8) are quite diversified for the two lines. In fact ERT A shows a heterogeneous near surface layer with resistivity between 20 and 50 Ωm. This covers a more conductive layer (resistivity of about 15 Ωm and thickness of 2-2.6 m) which can be interpreted as the saturated portion of the calcarenites; finally, a deep zone with resistivity between 25 and 45 Ωm related to the Ficarazzi clays. In ERT B the near surface layer shows higher resistivity (5-120 Ωm) related to the unsaturated calcarenites, and the conductive layer is clearly visible only in the western part, near a spring where water is collected in an underground cave, and the water level is attested at 2.5 m of depth. Differences of resistivity of the near surface layer can be related to a different supply of lake deposits.

The Induced Polarity results (fig. 9) show a chargeability distribution which generally follows that of the electrical resistivity, but differs from it in some areas, where, however, there were variations in the resistivity, even if less evident. IPT A shows a surface layer having a chargeability of about 10-20 ms overlying a layer with much higher chargeability (about 150 ms), which however decreases in the southwestern part, down to 30-40 ms. IPT B also shows a surface layer, but characterized by a less chargeability (6-10 ms), overlying a more heterogeneous layer, with chargeability from 30 to 80 ms. At the distance between 70 and 80 m there is a lower chargeability

anomaly, coinciding with a low resistivity zone in ERT B, which confirms the presence of the water concentration near the spring.

It can be seen that the results obtained by ERT and IPT are quite consistent with the images obtained by SRT.

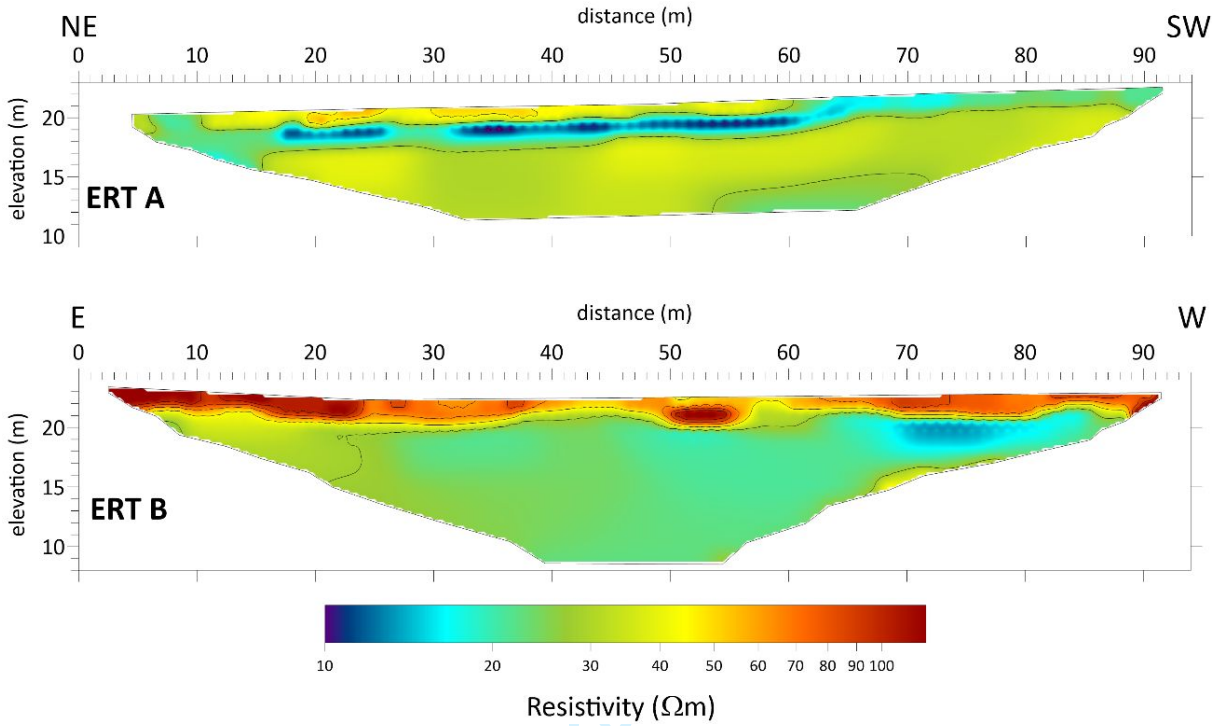

FIGURE 8: *Electrical Resistivity Tomographies in the Maredolce Lake.*

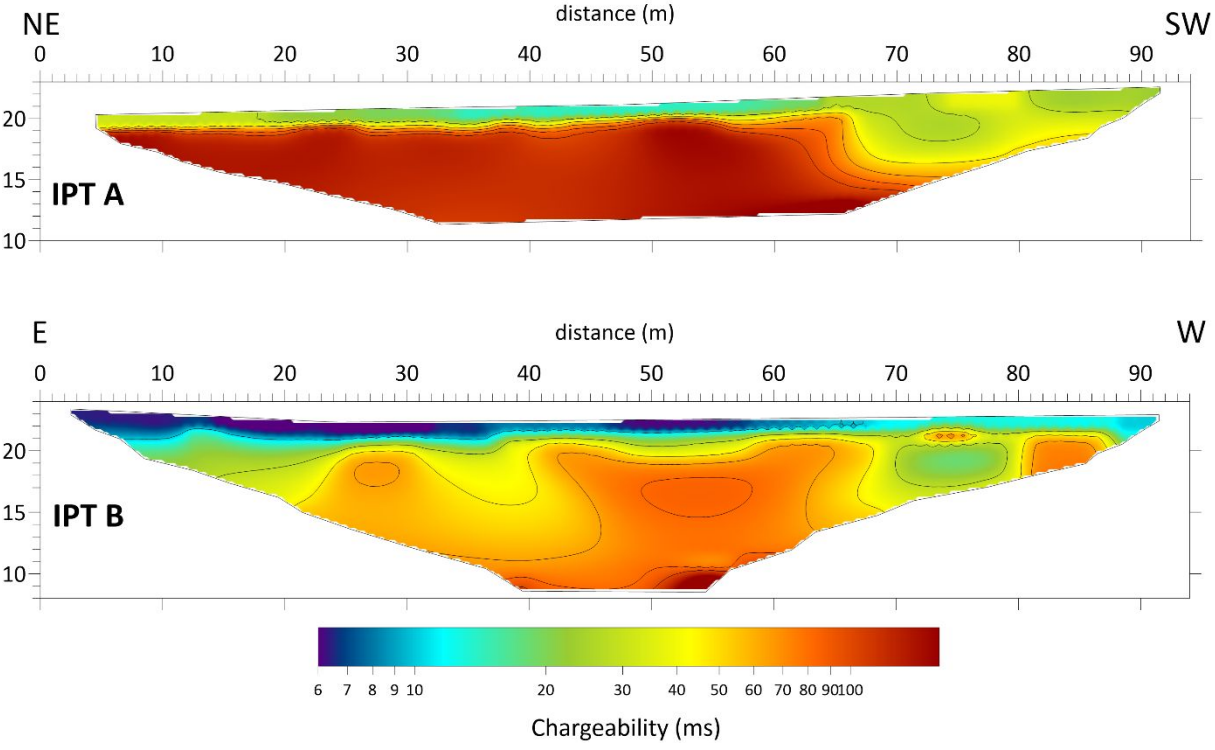

FIGURE 9: *Induced Polarization Tomographies in the Maredolce Lake.*

Multichannel Analysis of the Surface Waves

The MASW (Multichannel Spectral Analysis of Surface Waves) method (Park, Miller, & Xia, 1999) allows the evaluation of important mechanical characteristics of the soil through the analysis of the phenomenon of geometric dispersion of surface waves, in particular of Rayleigh waves. MASW is an active investigation technique. The dispersion occurs when there are variations in the elastic characteristics with carrying depth and, consequently, the different frequency components of a surface wave take on different speeds. In the MASW method seismic waves are generated by an artificial seismic source, generally a sledgehammer, and acquired through a linear array of equally spaced geophones placed on the surface. The seismograms acquired are analyzed in the frequency and wave number domain and from this a spectrum plot is obtained in which the spectral amplitudes are represented as a function of the phase velocity and frequency. By analyzing and picking the maximum spectral amplitudes, the dispersion curve of the fundamental mode of the Rayleigh waves is obtained and, if the clarity of the spectrum allows it, also the dispersion curves of the higher modes. Finally, from the inversion of the dispersion curves, a layered one-dimensional model of the shear waves velocity is obtained.

Two MASW surveys were carried out almost at the ends of the two tomographic lines, A and B (fig. 3), in order to obtain information on the shear waves velocity variation with depth in two different zones of the bottom of the ancient lake. Data measurements were made using 4.5 Hz geophones in number of 24, an intergeophonic distance of 2 m and a minimum offset between the first geophone and the source point of 5 m, considering the low velocity of the lake deposits. The seismic source was generated by hitting a metal plate placed on the ground with a sledgehammer weighing 8 kg. Acquired data have been analyzed and inverted by WinMasw software (Eliosoft, 2015). This software uses a genetic algorithm based inversion proposed by Dal Moro et al. (2007). Data analysis and inversion related to MASW1 survey (fig. 10), carried out close to tomography line A, shows a 2 m thick superficial layer with a S wave velocity equal to 230 m/s, followed downwards by an alternace of 2 m layer with velocity equal to 320 m/s. Below, there is a layer at a lower velocity (250 m/s), down to a depth of about 30 m, where the bedrock is located. Similar values were obtained from MASW2 survey carried out near tomography line B. Velocity relative to the near surface layers was used to constrain the HVSR investigations carried out at the bottom of the ancient artificial lake.

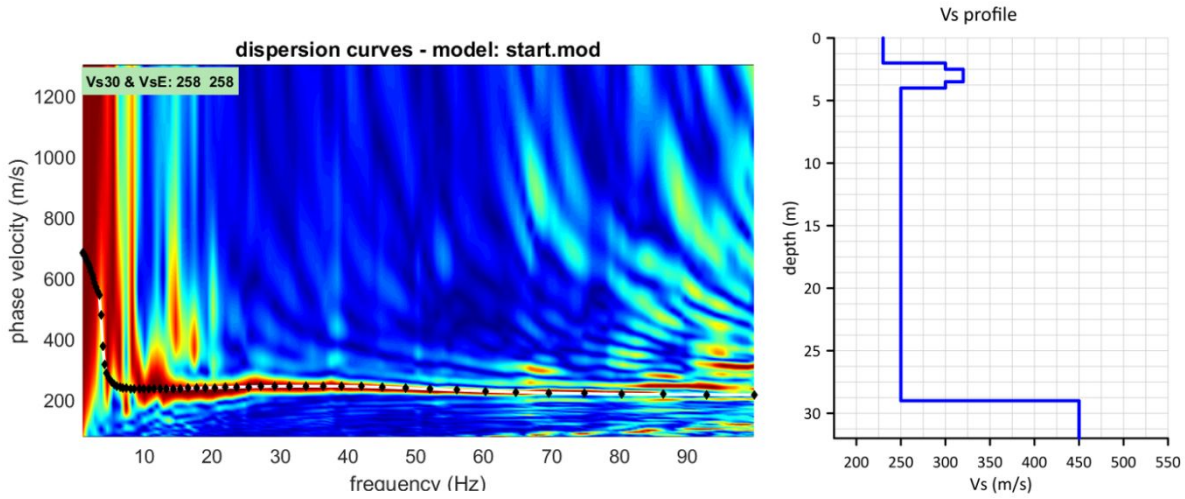

FIGURE 10: *Results of the MASW1 analysis realized at the end of tomography line A. Dispersion curve picking in the frequency-phase velocity domain (on the left) and Vs vertical profile obtained from the analysis (on the right).*

Ambient vibrations recording

The study of ambient seismic noise had great importance in defining the deep stratigraphy of the Maredolce site. Seismic noise is constituted by oscillations of amplitude which varies in a period range between 0.01 to 100 s (Asten, & Henstridge,1984). HVSR (Horizontal to Vertical Spectral Ratio) method is one of the main applications about seismic noise study. It was developed by Nakamura (1989) for the definition of the characteristics of the subsoil through the study of the environmental seismic noise (microtremors). A three-component broadband velocimeter measures vertical and two horizontal (north-south and east-west) components of ambient seismic noise, which includes microtremors induced by wind, ocean waves, and anthropogenic activity. The ratio of the averaged horizontal-to-vertical frequency spectrum, commonly referred to as H/V, is used to determine the fundamental site resonance frequency. Frequency peaks in the HVSR curve can be interpreted using regression equations to estimate sediment thickness and depth to bedrock.

Ambient noise registrations made and interpreted according to HVSR methodology are extremely useful, especially if assisted in their interpretations by information on the investigated site obtained from other survey methodologies such as perforations, other types of active and passive seismic surveys, laboratory tests of in situ samples, stratigraphic reconstructions of thicknesses. This information can act as a constraint to the inversion of HVSR data. For example, the MASW model can be used to limit the parameter search space for thickness and s-wave velocity of the most superficial layers in the HVSR inversion.

In the studied area 28 HVSR measurements have been performed to obtain information about sedimentary cover thickness and bedrock depth. Noise registrations were made using the Tromino®, a three-component broadband velocimeter with valid accuracy in the frequency range from 0.1 to about 30 Hz. The registration time chosen for each measurement was 20 minutes with a sampling frequency of 256 Hz. Two linear arrays were realized in the two depressed areas facing the castle, coinciding with the above discussed alignments A and B, including eight registration points per line. Along these arrays the distance between each recording station is about 15 m. Twelve other registration points were acquired to partially cover the entire surface of the ancient lake and the northern part of the islet. The data has been processed with the Grilla software (Micromed, 2011) which allows to perform the spectral analysis of the H/V ratio of the vertical and horizontal components recorded by the Tromino® and to invert the HVSR curves obtaining a one-dimensional subsoil model.

From the data analysis (fig. 11) an amplification peak is clear, at low frequencies between 1 and 2.4 Hz in all the HVSR curves. Moreover, a velocity inversion (H/V<1) is evident from 10 Hz down to 4 Hz. These or similar trends are also found in HVSR curves acquired in nearby zones, characterized by similar stratigraphic sequence. (Martorana, Agate, Capizzi, Cavera, & D'Alessandro, 2018). To overcome the equivalence limits of HVSR inverse problem (Dal Moro, 2014), HVSR inversions were constrained by MASW models and by cluster analysis of SRT and ERT (see the following chapter for more details).

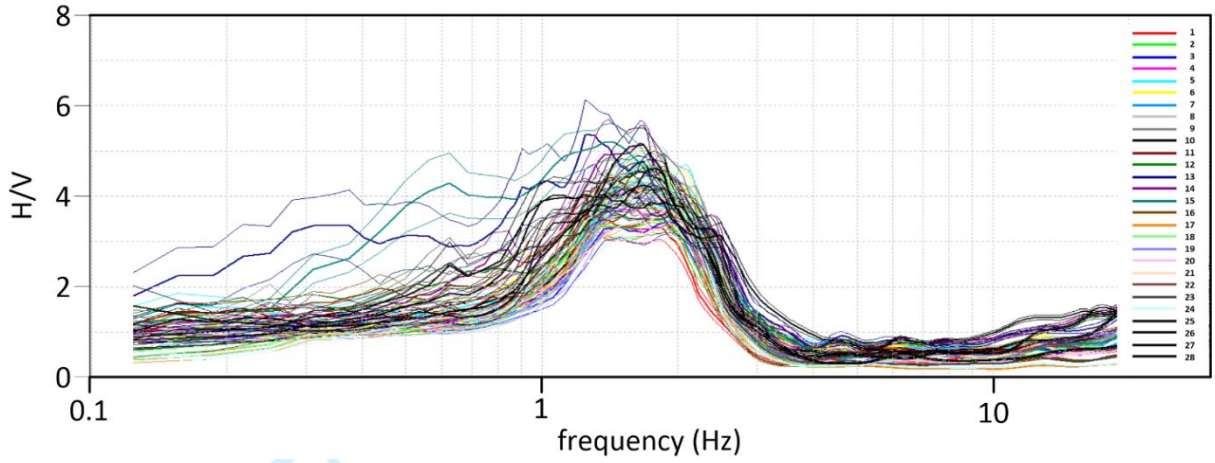

FIGURE 11: *Representation of the HVSR curves obtained from the 28 microtremors acquisitions in Maredolce site.*

Inverse models related to HVSR measurements made on the bottom of the ancient lake, show a cover layer with S wave velocity of about 230 m/s and average thickness from 1.4 m to 3.2 m, representative of the lake deposits. The layer below, with S wave velocity between 370 and 410 m/s and thickness varying from 1.4 m to 5 m can be interpreted as the Palermo calcarenites. Even lower, the inversion velocity (about 325 m/s) testify the presence of the Ficarazzi clays, considered an impermeable substrate. The fundamental peak, showed by all the curves, allowed to estimate the stratigraphic boundary between the Ficarazzi clays and the seismic bedrock, obtaining for the clays an average thickness of 45 m.

Considering the HVSR carried out on the calcarenitic bench that borders the deepest portions of the lake, calcarenites have a greater thickness (about 5 m) and the covering layer stands around 1.7 m This heterogeneous cover, a mix of lake, alluvial and agricultural deposits (Tullio, 1997), is characterized by S wave velocity of about 250 m/s. Finally, in two measurements made on the islet the first layer of about 1,3 m corresponds to superficial red soils and the calcarenites have a thickness of about 6 m.

Joint interpretation and construction of a 3D stratigraphic model of the subsoil

SRT and ERT performed were joint-interpreted using a cluster analysis method aimed at separating the subsoil into distinct areas (clusters) characterized by similar trends in the geophysical parameters considered (Gallardo, & Meju, 2003, Carollo, Capizzi, & Martorana, 2020). Cluster analysis is a multivariate analysis technique in which statistical units can be combined using an optimization criterion, minimizing the parametric distance within each group and at the same time maximizing it. The parametric distance is quantified by measures of similarity and / or dissimilarity between defined statistical units. Thus, with the cluster analysis method, it is possible to identify within a set of parameters some clusters, based on their level of similarity (Barbarito, 1999). In this work, a statistical approach based on non-hierarchical cluster analysis (k-means) has been applied (Di Giuseppe, Troiano, Troise, & De Natale, 2014; Capizzi et al., 2017), The cluster analysis was performed on static units defined by electrical resistivity values, P wave velocities, and seismic density on coincident sections (Carollo, Capizzi, & Martorana, 2020. A re-discretion of the meshes of the electric and seismic tomographies was carried out, to obtain a unique refined mesh, which was inscribed in both boundaries of the models. In this way it was possible for each cell of the refined mesh a set of geophysical parameters (electrical resistivity, seismic p wave velocity, seismic ray density). The results of cluster analysis are showed in fig. 12.

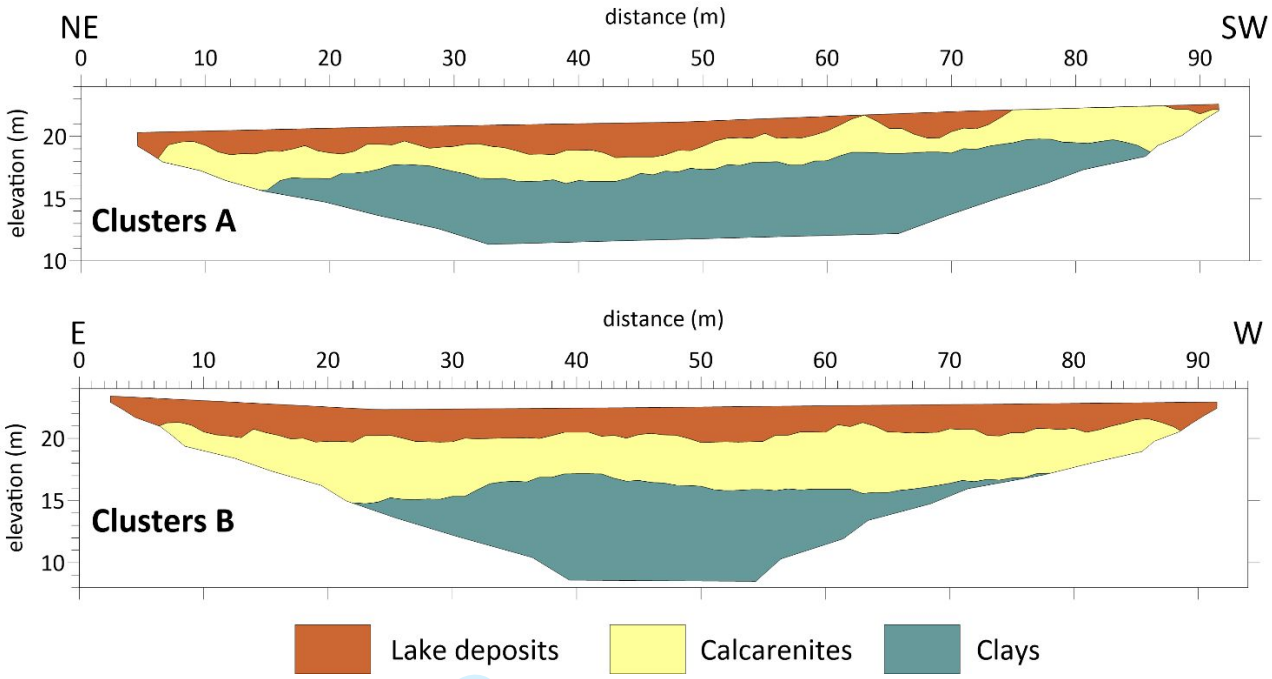

FIGURE 12: *Results of the cluster analysis applied to ERT A and SRT A (top) and to ERT B and SRT B (bottom).*

For both sections a number of clusters equal to three was considered, with the aim of representing the three lithologies recognized thanks also to the information derived from stratigraphic data catalogued in the cityGIS database (Giammarinaro, Canzoneri, Vallone, & Zuccarello, 2003; Giammarinaro, Maiorana, & Vallone, 2003). In particular, the wells 0433 and 1198 were considered (fig. 3). Hence the first layer represents lake deposits of Capo Playa Synthem, the second layer the Palermo calcarenites, and the third Ficarazzi Clays. It is noted that lake deposits are not always present, and have thicknesses ranging from 0 to 5 m approximately. In section A (fig. 12, top) the thickness of the calcarenites is lower (from 2 to 4 m) and the layer is updip towards SW. Also, the top of the Ficarazzi Clays is updip towards NW with an altitude ranging from 15 to 20 m. In section B (fig. 12, bottom) the thickness of the calcarenites is greater (from 3 to 6 m) and the layer appears sub-horizontal. The top of the Ficarazzi clays stands between about 15 and 17 m.

Some microtremor measurements were performed in almost alignment with the electric and seismic tomographies (measurements 1-8 for line A and measures 9-16 for line B). The HVSR curves for these measurements have been inverted using as constraints both the S waves velocity of the first layer obtained from the MASW models, and by imposing research spaces centered on the layer thicknesses indicated by the cluster analysis. The HVSR inverse models, thus constrained, showed thicknesses that differ from those indicated by the cluster analysis for less than 0.5 m. Subsequently, HVSR curves 17 to 28 have been inverted by imposing constraints of lateral continuity. In this way the constrained inversions of the HVSR curves allowed to estimate the depth of a seismic bedrock, indicated by the peak frequency of 1-2.4 Hz present in each curve. This bedrock is characterized by Vs values generally greater than 800 m/s and is interpretable as the stratigraphic contact between the Ficarazzi clays and the quartzarenite member of the Numidian Flysch (Catalano et al., 2013).

In order to generate a 3D stratigraphic model, all the geophysical models, together with the stratigraphic data obtained from the wells in the area, were organized in a database from which the stratigraphic surfaces were obtained by kriging interpolation using Surfer software. For the topographical surface a Digital Elevation Model was used, with a resolution of 1 m.

Figure 13 shows two vertical sections with directions E-W and N-S obtained from the aforementioned model, which show how lake deposits are found only in some areas of the lake,

while the calcarenites have overall a downdip towards the north. For scaling problems, the sections have been cut down to 0 m asl, even if the 3D model obtained deepens up to the contact between the Ficarazzi clays and the Numidian Flysch, which is located at altitudes between -25 and -28 m asl.

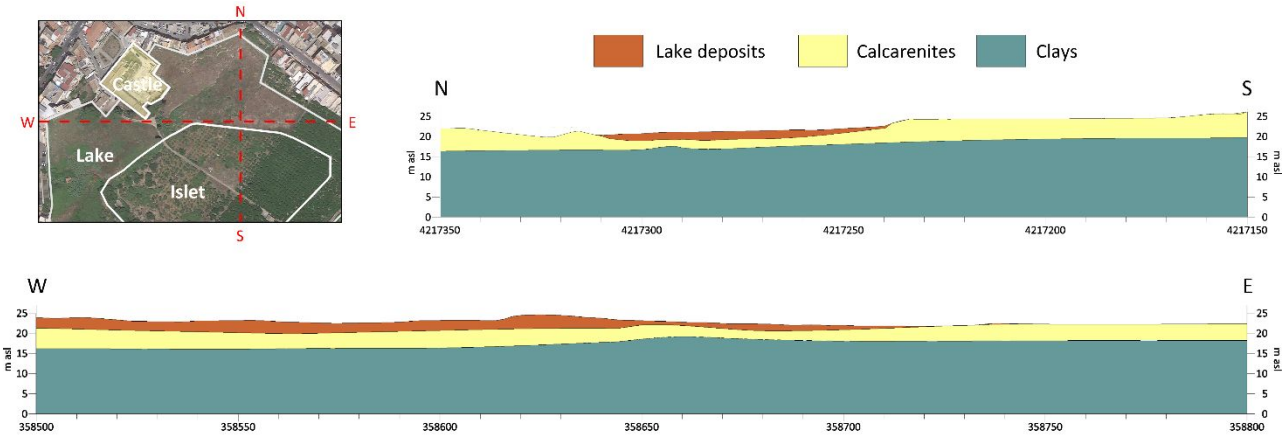

FIGURE 13: *Vertical sections with directions N-S (top) and E-W (bottom) obtained from the 3D-stratigraphical model of the subsoil of the Maredolce Lake.*

The maps of the thicknesses of the represented lithotypes have been obtained from the stratigraphic surfaces of the 3D model and are plotted as isopach maps. Figures 14 show that lake deposits are limited in the two depressed areas where tomographic surveys were made. In particular, in zone A these deposits have smaller thicknesses, between 0 and 2 m, while in zone B they range from 2 to 3 m.

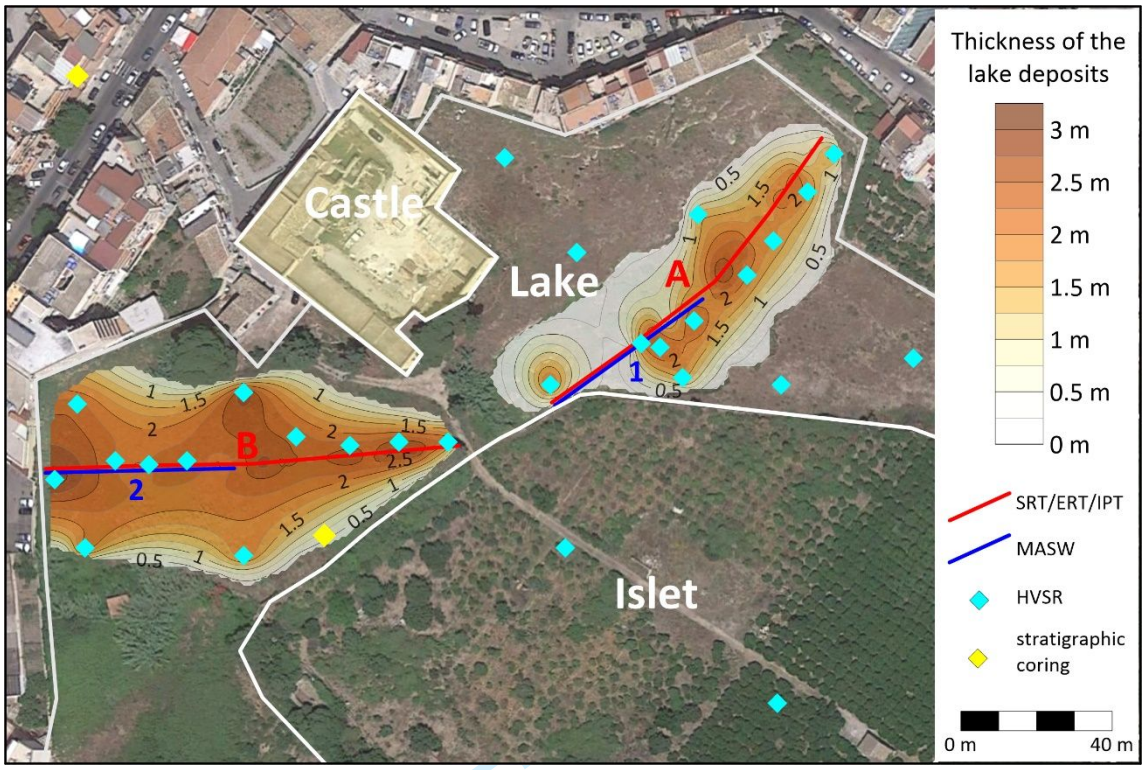

FIGURE 14: *Isopach map of the lake deposits in the subsoil of the Maredolce Lake.*

The isopach map of the calcarenites (fig. 15) shows thickness varying from about 1 to 7 m, less in the lake area than in the islet and peripheral areas. In particular, within the lake, there is a limited zone near the center of line A, where the thicknesses are very small, between 1 and 2 m.

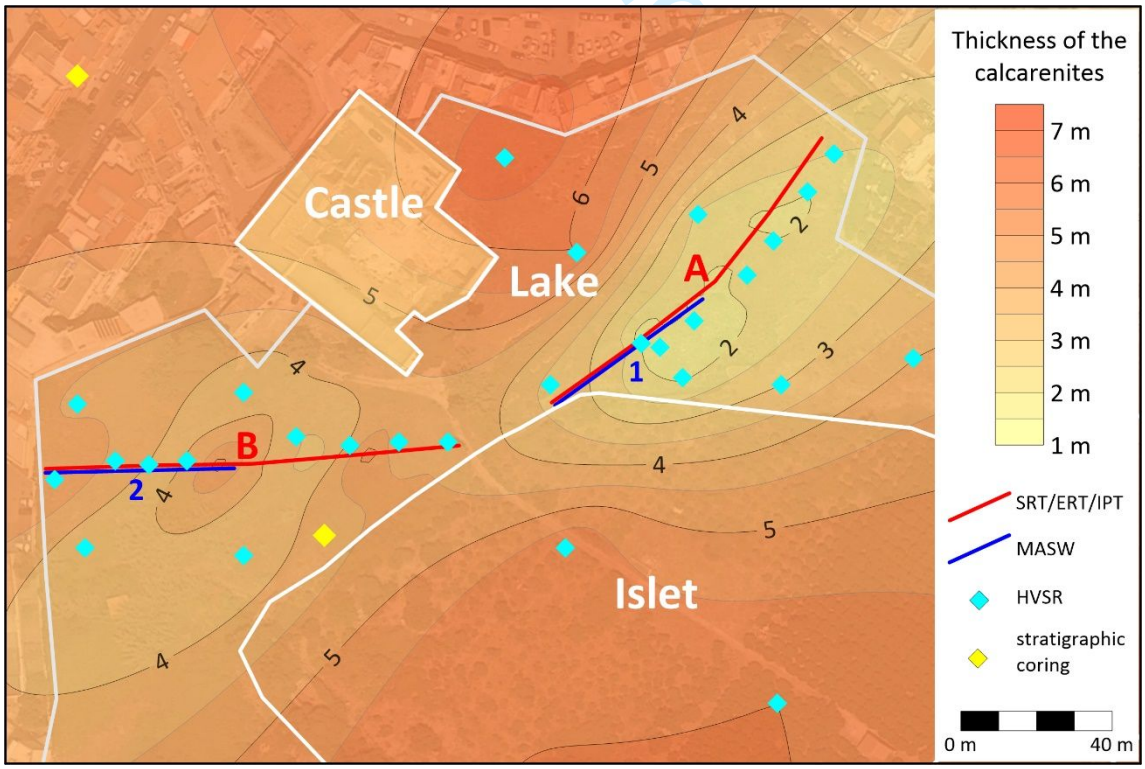

FIGURE 15: *Isopach map of the Palermo calcarenites in the subsoil of the Maredolce Lake.*

Finally, the isopach map of the Ficarazzi clays (fig. 16) does not show significant variation of its thickness, which is between about 42 and 48 m.

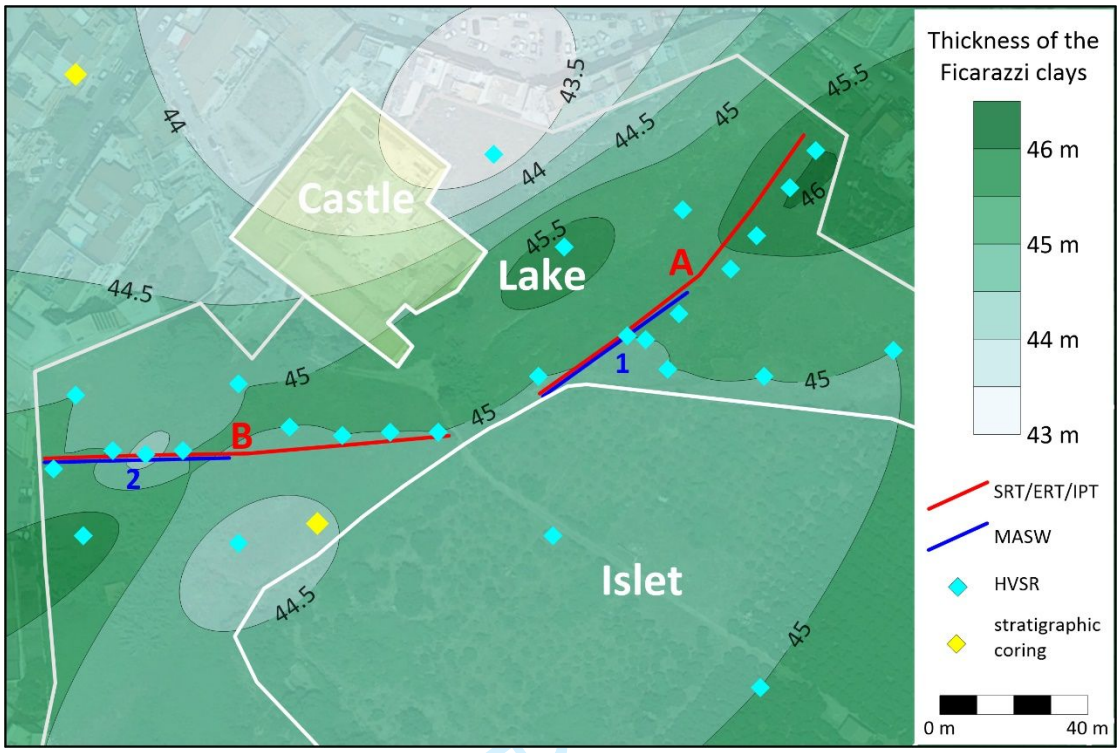

FIGURE 16: *Isopach map of the Ficarazzi Clays in the subsoil of the Maredolce Lake.*

Geotechnical modeling and implications for the project

From the interpretation of the results obtained with the geophysical investigations in the context of this study, it emerges that the soils present in the area that must be affected by the waters of the artificial lake are, from top to bottom:

- the Holocene lake deposits (Capo Plaia Syntem);
- the Pleistocene Palermo calcarenites, in mainly calcarenitic facies, affected by mostly sub-vertical joints and by sub-horizontal bedding planes;
- the Ficarazzi Clays (lower Pleistocene);
- the Numidian Flysch, in mainly clay facies ("ginolfo") of the upper Oligocene - lower Miocene.

The lake deposits are made up of alternations, in sub-horizontal layers of modest thickness, of fine sand levels, sometimes silty, with rare elements of gravel with rounded edges, and clay silt, at peaty places (Contino, et al., 2006). This spatial configuration gives the material as a whole anisotropy with regard to permeability: in fact, in the vertical direction, orthogonal to the layers, the permeability k is close to that of the silty levels and stands at values of the order of 10–5 cm/s. On the contrary, the permeability in the horizontal direction, parallel to the layers, is close to that of the sandy levels, in the order of 10-2 cm/s. Taking into account, also, the irregularity of the spatial distribution of the levels with different granulometry, the lake deposits overall are characterized by average permeability, of the order of 10-3 cm/s.

The underlying Palermo Calcarenites, in which the nodular calcarenite facies prevails, is characterized by high permeability for both porosity and cracking and the average values of k are around 10-2 cm/s.

The permeability of the Ficarazzi Clays is strictly linked to the granulometric composition of the material, which has sandy-silty levels, distributed randomly, within the mainly pelitic material. By in situ permeability tests with variable load, averages of k around 10-6 cm/s were obtained, which do not vary significantly with the direction.

The permeability of the pelitic facies of the Numidian Flysch is closely linked to the scaly texture of the material, as shown by an experimental scientific research developed at the Universities of Palermo, Cosenza and Naples (Nocilla, & Umiltà, 1978; Bilotta, & Umiltà, 1981; Bilotta, Pellegrino, & Picarelli, 1985). In fact, the scalies constitute discontinuities that give the pelitic mass a secondary permeability by cracking, whose average values are generally close to 10-5 cm/sec.

The geotechnical model of the area under study is ultimately characterized by a first permeable horizon, comprising all the lake deposits and calcarenites, the thickness of which, in correspondence with the lake area, varies from about 3 m to about 7 m (fig. 17). It rests on the Ficarazzi Clays, which represents the least permeable horizon, with a thickness greater than 40 m (fig. 16), capable of guaranteeing a fair hydraulic seal over time.

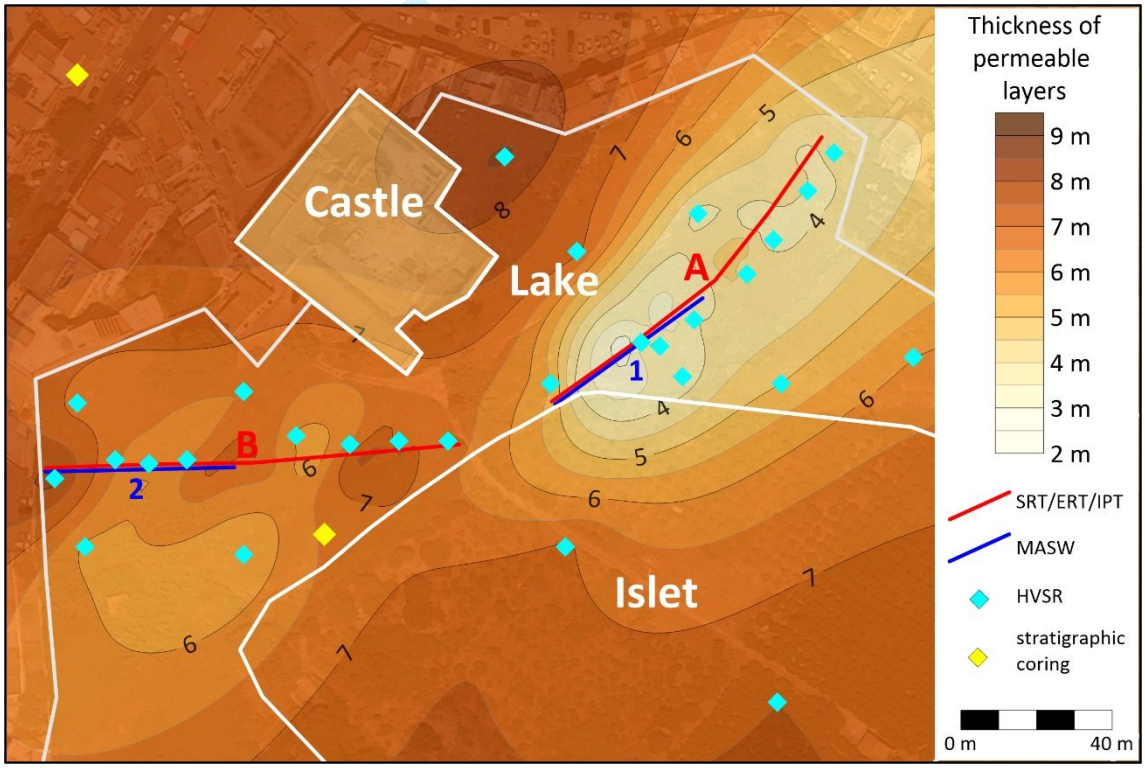

FIGURE 17: *Isopach map of the permeable layers in the subsoil of the Maredolce Lake.*

It is evident, in the illustrated geotechnical and hydraulic context, the need to guarantee the permanence of the lake with techniques of waterproofing the bottom, as the Normans had done using a "cocciopesto" hydraulic plaster already nine centuries ago, when the lake was still fed naturally by the source of the Favara, which guaranteed just under 70 l/s. At present the source, exploited for the needs of the city of Palermo, has been diverted so that in the area under study there is only a seasonal stratum, located in the calcarenitic complex, absolutely inadequate for a continuous feeding of the lake.

The thickness and the specific lithostratigraphic and geotechnical characteristics of the permeable surface soils make the hypothesis of a waterproofing treatment impossible. In fact, the available technologies are effective in the local reduction of permeability by porosity, proving to be completely inadequate in the case of permeability by cracking, as in calcarenites, and of anisotropy of permeability by stratification in pelitic soils, as in holocene lake deposits. In addition, in this

specific case the problem is even more complex due to the thickness of the complex of permeable soils (lake deposits + calcarenites), which in the area of the artificial lake also reaches values of several meters (fig. 17).

Hence the need to waterproof the bottom of the artificial lake with adequate techniques, whose primary feature, in addition to the hydraulic seal, must be compatibility with the environment, as they must allow the development of native vegetation, fish and insects, recreating the natural microclimate of lakes and ponds. With this in mind, multidisciplinary studies of geotechnical and environmental engineering, botany, ecology, architecture are underway to identify the solution capable of optimizing technical and environmental problems.

Conclusions

From a geotechnical point of view, on the basis of the results acquired with geophysical investigations and borrowed from the literature (laboratory and in situ tests), the waterproof horizon was identified in the Ficarazzi Clays, capable of ensuring hydraulic seal. The possibility of interventions aimed at reducing the permeability of the overlying lands (lake and calcarenite deposits), of about 2 orders of magnitude, was therefore assessed without success.

In fact, the permeability of these materials is complex and not just for porosity: in particular it is mainly linked to discontinuities of exclusively stratigraphic origin, for recent soils, stratigraphic and tectonic, for calcarenites. In addition, with the investigations developed for this work, a significant variability in the thickness of the permeable soils in the area of interest has been identified, with maximum values of about 7 m, which however makes any waterproofing treatment impossible. The ongoing studies are therefore directed to the choice of the most appropriate material to be placed on the bottom of the area to be flooded to ensure its hydraulic seal while respecting the environment.

The first results seem to confirm that the best waterproofing technique for the lake bottom is the use of bentonite geocomposites, consisting of a double layer of geotextile with bentonite inside; the same bentonite is used for welding the contacts between the individual adjacent panels. This technique has been successfully applied for waterproofing the bottom of existing lakes and for the construction of new bodies of water in the WWF oasis of the "Vanzago forest" (Milan), where detailed monitoring of the effectiveness of the system used in the water tightness and protection and reconstitution of the aquatic habitat is underway.

References

Abate, B., Catalano, R., & Renda, P. (1978). Schema geologico dei monti di Palermo (Sicilia). *Bollettino della Società Geologica Italiana,* 97, 807-819.

Agate, M., Basilone, L., Di Maggio, C., Contino, A., Pierini, S., & Catalano, R. (2017). Quaternary marine and continental unconformity-bounded stratigraphic units of the NW Sicily coastal belt. Journal of Maps, 13, 2, 425-437. (Open Access).

Amari, M. (1939). Storia dei Musulmani di Sicilia, ed. a cura di Carlo Alfonso Nallino, 5 voll., Catania, Prampolini, 1933-1939.

Asten, M. W., & Henstridge, J. D. (1984). Array estimators and use of microseisms for reconnaissance of sedimentary basins. *Geophysics*, 49(11), pp. 1828-1837. https://doi.org/10.1190/1.1441596.

Barbarito, L. (1999). L'analisi di settore: metodologia e applicazioni, Milano, Franco Angeli Ed.

Barbera, G., Boschiero, P., & Latini, L. (2015). Maredolce - La Favara. Premio Internazionale Carlo Scarpa per il Giardino 2015. XXVI edizione, Fondazione Benetton Studi Ricerche, Treviso 2015. ISBN 978-88-97784-70-8.

Bilotta, E., Pellegrino, A., & Picarelli, L. (1985). Geotechnical properties and slope stability in

structurally complex clay soils. In: *Geotechnical Engineering in Italy.* An Over view pp. 195-214 Associazione Geotecnica Italiana, Roma.

Bilotta, E., & Umiltà, G. (1981). Indagini sperimentali sulla resistenza a rottura di argille a scaglie. *Rivista Italiana di Geotecnica*, n, 1, pp. 15-26.

Capizzi, P., Martorana, R., Carollo, A., & Vattano, M. (2017). Cluster analysis for cavity detection using seismic refraction and electrical resistivity tomography. *In 23rd European Meeting of Environmental and Engineering Geophysics,* (Vol. 2017, No. 1, pp. 1-5). European Association of Geoscientists & Engineers. We 23P2 23. https://doi.org/10.3997/2214-4609.201702123.

Cardarelli, E., & Di Filippo, G. (2004). Integrated geophysical surveys on waste dumps: Evaluation of physical parameters to characterize an urban waste dump (four case studies in Italy). *Waste Management & Research*, vol. 22, no. 5, pp. 390-402. https://doi.org/10.1177/0734242X04046042.

Carollo A., Capizzi P., Martorana R. (2020). Joint interpretation of seismic refraction tomography and electrical resistivity tomography by cluster analysis to detect buried cavities. *Journal of Applied Geophysics*, 2020, 104069, ISSN 0926-9851. https://doi.org/10.1016/j.jappgeo.2020.104069.

Catalano, R., Avellone, G., Basilone, L., Contino, A., & Agate M. (2013). Note illustrative della Carta Geologica d'Italia del foglio 595 "Palermo" e carta geologica, scala 1:50.000. Regione Siciliana - Ispra.

Chirindja, F. J., Dahlin, T., Juizo, D., & Steinbruch, F. (2017). Reconstructing the formation of a costal aquifer in Nampula province, Mozambique, from ERT and IP methods for water prospection. *Environmental Earth Sciences*, vol. 76, no. 1, 36. https://doi.org/10.1007/s12665-016-6364-0.

Coggon, J. H. (1971). Electromagnetic and electrical modeling by the finite element method. *Geophysics* 36(1): 132–155. https://doi.org/10.1190/1.1440151.

Contino, A., Giammarinaro, M. S., Vallone, P., Varsalona, S., & Zuccarello, A. (2006). Analisi stratigrafico geotecnica del settore meridionale della citta di Palermo finalizzata alla caratterizzazione di fattori di pericolosita sismica in esso presenti. Bollettino-Societa Geologica Italiana, 125(3), 329.

Dal Moro, G. (2014). Surface wave analysis for near surface applications. Elsevier.

Dal Moro, G., Pipan, M., & Gabrielli, P. (2007) Rayleigh wave dispersion curve inversion via genetic algorithms and Marginal Posterior Probability Density estimation. *Journal of Applied Geophysics,* 61(1), 39-55.

De Domenico, D., Giannino, F., Leucci, G., & Bottari, C. (2006). Integrated geophysical surveys at the archaeological site of Tindari (Sicily, Italy). *Journal of Archaeological Science*, vol. 33, no. 7, pp. 961-970. https://doi.org/10.1016/j.jas.2005.11.004.

Deiana, R., Leucci, G., & Martorana, R. (2018). New perspectives on geophysics for archaeology: A special issue. *Surveys in Geophysics*, 39(6), 1035-1038. https://doi.org/10.1007/s10712-018-9500-4

Dey, A., & Morrison, H. F. (1979). Resistivity modelling for arbitrary shaped two-dimensional structures. *Geophysical Prospecting,* 27(1): 106–136. https://doi.org/10.1111/j.1365-2478.1979.tb00961.x.

Di Giuseppe, M. G., Troiano, A., Troise, C., & De Natale, G. (2014). K-means clustering as tool for multivariate geophysical data analysis. *An application to shallow fault zone imaging. J. Appl. Geophys*. 101, 108–115. https://doi.org/10.1016/j.jappgeo.2013.12.004.

Eliosoft. (2015). Geophysical software and services. WinMASW 7.0 User manual.

Gallardo, L. A., & Meju, M. A. (2003). Characterization of heterogeneous near-surface materials by joint 2D inversion of dc resistivity and seismic data. *Geophysical Research Letters*, 30(13). https://doi.org/10.1029/2003GL017370.

Gebrande, H., & Miller, H. (1985). Refraktionsseismik. In: *Angewandte Geowissenschaften II*. Ferdinand EnkeVerlag, Stuttgart, 226-260. ISBN: 3-432-91021-5.

Giammarinaro, M. S., Canzoneri, V., Vallone, P., & Zuccarello, A. (2003). Effects of the September 6th, 2002 earthquake: damage amplification in the south-eastern sector of Palermo explained through GIS technology. *Annals of Geophisics*, Vol 46 n.6, pp. 1195-1207. https://doi.org. 10.4401/ag-3466.

Giammarinaro, M. S., Maiorana, S., Vallone, P. (2003). A GIS application for Historical-Monumental Heritage. Proceedings 4th European Congress on Regional Geoscientific Carthography and Information Systems, Volume I.

Gibelli, G. M., & Pirrera, G. (2017). Piano Integrato della Riserva Naturale Regionale "Bosco WWW di Vanzago".

Gibson, B. S., Odegard, M. E., & Sutton, G. H. (1979). Nonlinear least-squares inversion of traveltime data for a linear velocity-depth relationship. *Geophysics*, 44(2), 185-194. http://dx.doi.org/10.1190/1.1440960.

Gonzales Amaya, A., Dahlin, T., Barmen, G., & Rosberg, J. E. (2016). Electrical resistivity tomography and induced polarization for mapping the subsurface of alluvial fans: A case study in Punata (Bolivia). *Geosciences* (Switzerland), 6(4), 51. https://doi.org/10.3390/geosciences6040051.

Grandjean, G., Gourry, J. C., Sanchez, O., Bitri, A., & Garambois, S. (2011). Structural study of the Ballandaz landslide (French Alps) using geophysical imagery. *Journal of Applied Geophysics*, 75(3), 531–542. https://doi.org/10.1016/j.jappgeo.2011.07.008.

Griffiths, D. H., & Barker, R. D. (1994). Electrical imaging in archaeology. *Journal of Archaeological Science*, 21 (2), 153–158. https://doi.org/10.1006/jasc.1994.1017.

Kemna, A., Binley, A., Cassiani, G., Niederleithinger, E., Revil, A., Slater, L., Williams, K. H., Orozco, A.F., Haegel, F. H., Hoerdt, A., Kruschwitz, S., Leroux, S., Titov, K., & Zimmermann, E. (2012). An overview of the spectral induced polarization method for near-surface applications. *Near Surface Geophysics* 10(6), 453–468. https://doi.org/10.3997/1873-0604.2012027.

Koch, K., Wenninger, J., Uhlenbrook, S., & Bonell, M. (2009). Joint interpretation of hydrological and geophysical data: Electrical resistivity tomography results from a process hydrological research site in the Black Forest Mountains, Germany. *Hydrological Processes: An International Journal*, vol. 23, no. 10, pp. 1501-1513. https://doi.org/10.1002/hyp.7275.

Lapenna, V., Lorenzo, P., Perrone, A., Piscitelli, S., Sdao, F., & Rizzo, E. (2003). High-resolution geoelectrical tomographies in the study of Giarrossa landslide (southern Italy). *Bulletin of Engineering Geology and the Environment,* 62(3), 259–268. https://doi.org/10.1007/s10064-002-0184-z.

Lehmann, P., Gambazzi, F., Suski, B., Baron, L., Askarinejad, A., Springman, S. M., Holliger, K., & Or, D. (2013). Evolution of soil wetting patterns preceding a hydrologically induced landslide inferred from electrical resistivity survey and point measurements of volumetric water content and pore water pressure. *Water Resources Research,* 49(2), 7992–8004. https://doi.org/10.1002/2013WR014560.

Loke, M.H., 2013. Tutorial: 2-D and 3-D Electrical Imaging Surveys. www.geotomosoft.com.

Loke, M. H., Wilkinson, P. B., Chambers, J. E., Uhlemann, S. S., & Sorensen, J. P. R. (2015). Optimized arrays for 2-D resistivity survey lines with a large number of electrodes. *Journal of Applied Geophysics*, 112, 136-146. https://doi.org/10.1016/j.jappgeo.2014.11.011.

Loke, M. H., Acworth, I., & Dahlin, T. (2003). A comparison of smooth and blocky inversion methods in 2D electrical imaging surveys. *Exploration Geophysics*, 34(3): 182–187. https://doi.org/10.1071/EG03182.

Martorana, R., Agate, M., Capizzi, P., Cavera, F., & D'Alessandro, A. (2018). Seismo-stratigraphic model of "La Bandita" area (Palermo Plain, Sicily) through HVSR inversion constrained by stratigraphic data. *Italian Journal of Geosciences*, 137, 1, 73-86. https://doi.org/10.3301/IJG.2017.18.

Martorana, R., Capizzi, P., D'Alessandro, A., & Luzio, D. (2017). Comparison of different sets of array configurations for multichannel 2D ERT acquisition. *Journal of Applied Geophysics,* 137, 34–48. https://doi.org/10.1016/j.jappgeo.2016.12.012. ISSN: 0926-9851.

Martorana, R., Lombardo, L., Messina, N. & Luzio, D. (2014). Integrated geophysical survey for 3D modelling of a coastal aquifer polluted by seawater. *Near Surface Geophysics*, vol. 12, no. 1, pp. 45-59. https://doi.org/10.3997/1873-0604.2013006.

Merritt, A. J., Chambers, J. E., Murphy, W., Wilkinson, P. B., West, L. J., Gunn, D. A., Meldrum, P. I., Kirkham, M., & Dixon, N. (2014). 3D ground model development for an active landslide in Liasmudrocks using geophysical, remote sensing and geotechnical methods. *Landslides,* 11(4), 537–550. https://doi.org/10.1007/s10346-013-0409-1.

Micromed. (2011). Dati tecnici Tromino e download pacchetto software Grilla. Disponibile online all'indirizzo http://www.tromino.it.

Nakamura, Y. (1989). A method for dynamic characteristics estimation of subsurface using microtremor on the ground surface. *Quarterly report Railway Technical Research Institute*, 30(1).

Nocilla, N., & Umiltà, G. (1978). Caratterizzazione geotecnica del terreno di fondazione di una diga in Sicilia. Proc. *13th Natl Mtg on Geotechnics*, Merano.

Okay, G., Leroy, P., Ghorbani, A., Cosenza, P., Camerlynck, C., Cabrera, J., Florsch, N., & Revil, A. (2014). Spectral induced polarization of clay-sand mixtures: Experiments and modeling. *Geophysics*, vol. 79, no. 6, pp. E353-E375. https://doi.org/10.1190/geo2013-0347.1.

Park, C.B., Miller, R.D., & Xia, J. (1999). Multichannel analysis of surface waves. *Geophysics,* 64(3), 800–808, doi: https://doi.org/10.1190/1.1444590.

Pidlisecky, A., Haber, E., & Knight, R. (2007). RESINVM3D: a 3D resistivity inversion package. *Geophysics*, 72(2): H1–H10. https://doi.org/10.1190/1.2402499.

Rawlinson, N., Pozgay, S., & Fishwick, S. (2010). Seismic tomography: a window into deep Earth. *Physics of the Earth and Planetary Interiors,* 178 (3-4), 101-135. https://doi.org/10.1016/j.pepi.2009.10.002.

Revil, A., & Glover, P. W. J. (1998). Nature of surface electrical conductivity in natural sands, sandstones, and clays. *Geophysical Research Letters*, 25(1), 691-694. https://doi.org/10.1029/98GL00296.

Robert, T., Dassargues, A., Brouyère, S., Kaufmann, O., Hallet, V., & Nguyen, F. (2011). Assessing the contribution of electrical resistivity tomography (ERT) and self-potential (SP) methods for a water well drilling program in fractured/karstified limestones. *Journal of Applied Geophysics*, vol. 75, no. 1, pp. 42-53. https://doi.org/10.1016/j.jappgeo.2011.06.008.

Rohdewald, S.R. (2011). Interpretation of first-arrival travel times with wavepath Eikonal traveltime inversion and wavefront refraction method. *In Symposium on the Application of Geophysics to Engineering and Environmental Problems 2011* (pp. 31-38). Society of Exploration Geophysicists. https://doi.org/10.4133/1.3614086.

Schuster, G. T., & Quintus-Bosz, A. (1993). Wavepath Eikonal traveltime inversion: Theory. *Geophysics, 58*(9), 1314-1323. http://dx.doi.org/10.1190/1.1443514.

Slater, L., Ntarlagiannis, D., & Wishart, D. (2006). On the relationship between induced polarization and surface area in metal-sand and clay-sand mixtures. *Geophysics*, vol. 71, no. 2, pp. A1-A5. https://doi.org/10.1190/1.2187707.

Todaro, P. (2016). Aspetti geomorfologici, idrologici ed idraulici del lago medievale di Maredolce a Palermo. *Geologia dell'ambiente 3, 2016 - Italian Magazine of Environmental Geology, 3-12.*

Todaro, P. (2015). Maredolce - La Favara - La natura del luogo: aspetti geomorfologici, idrologici e idraulici dell'antica Favara di Maredolce a Palermo. Premio Internazionale Carlo Scarpa per il Giardino 2015, XXVI edizione, Fondazione Benetton Studi Ricerche, Treviso 2015 (135-145).

Trapani, F. (2014). Maredolce: studiare il territorio di Maredolce/Brancaccio e valorizzarlo come distretto culturale e turistico. *Quaderni di Maredolce*. Maredolce: una centralità nuova nella porta meridionale di Palermo, Amici di Plumelia. ISBN: 978-88-98731-91-6.

Tsokas, G. N., Tsourlos, P. I., Vargemezis, G., & Novack, M. (2008). Non-destructive electrical resistivity tomography for indoor investigation: the case of Kapnikarea church in Athens. *Archaeological Prospection*, 15(1), 47–61. https://doi.org/10.1002/arp.321.

Tullio, A. (1997). Strumenti per la lavorazione dello zucchero a Maredolce (Palermo). In Archeologia e territorio, Palermo, pp. 471-479.

Figure Captions

FIGURE 1: *Elements of the Favara-Maredolce monumental complex.*

FIGURE 2: *The Castle of Maredolce: a) the main facade with the three entrances; b) the palace seen from the lake; c) the chapel of Saints James and Philip; d) the hemispherical dome of the chapel; e) the muqarnas and f) the pleated vault of royal hall.*

FIGURE 3: *Aerial photo of the monumental complex of Maredolce, with the locations of the geophysical surveys carried out and the core drillings.*

FIGURE 4: *Surveying scheme of the Seismic Refraction Tomographies (top) and an example of seismograms related to the shot 5 of the SRTA (bottom), showing the picking of the first arrival times.*

FIGURE 5: *Seismic Refraction Tomography line A: P-waves velocity (top) and raypath density (bottom).*

FIGURE 6: *Seismic Refraction Tomography line B: P-waves velocity (top) and raypath density (bottom).*

FIGURE 7: *Pattern of the relative sensitivity of the electrical resistivity tomographies carried out in the Maredolce Lake.*

FIGURE 8: *Electrical Resistivity Tomographies in the Maredolce Lake.*

FIGURE 9: *Induced Polarization Tomographies in the Maredolce Lake.*

FIGURE 10: *Results of the MASW1 analysis realized at the end of tomography line A. Dispersion curve picking in the frequency-phase velocity domain (on the left) and Vs vertical profile obtained from the analysis (on the right).*

FIGURE 11: *Representation of the HVSR curves obtained from the 28 microtremors acquisitions in Maredolce site.*

FIGURE 12: *Results of the cluster analysis applied to ERT A and SRT A (top) and to ERT B and SRT B (bottom).*

FIGURE 13: *Vertical sections with directions N-S (top) and E-W (bottom) obtained from the 3D-stratigraphical model of the subsoil of the Maredolce Lake.*

FIGURE 14: *Isopach map of the lake deposits in the subsoil of the Maredolce Lake.*

FIGURE 15: *Isopach map of the Palermo calcarenites in the subsoil of the Maredolce Lake.*

FIGURE 16: *Isopach map of the Ficarazzi Clays in the subsoil of the Maredolce Lake.*

FIGURE 17: *Isopach map of the permeable layers in the subsoil of the Maredolce Lake.*

FIGURE 1: Elements of the Favara-Maredolce monumental complex.

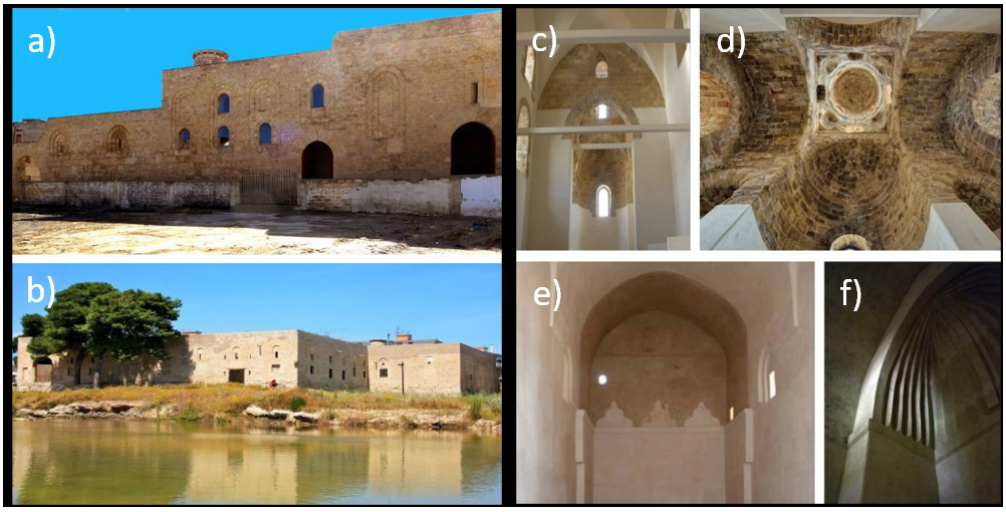

FIGURE 2: The Castle of Maredolce: a) the main facade with the three entrances; b) the palace seen from the lake; c) the chapel of Saints James and Philip; d) the hemispherical dome of the chapel; e) the muqarnas and f) the pleated vault of royal hall.

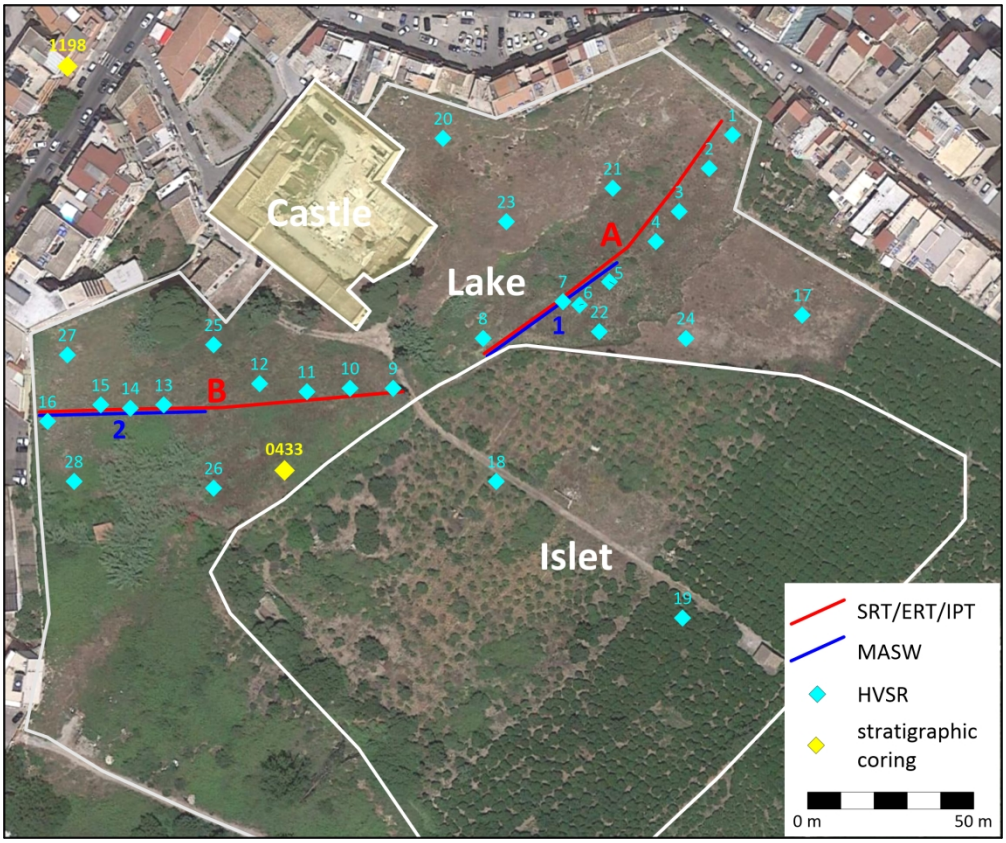

FIGURE 3: Aerial photo of the monumental complex of Maredolce, with the locations of the geophysical surveys carried out and the core drillings.

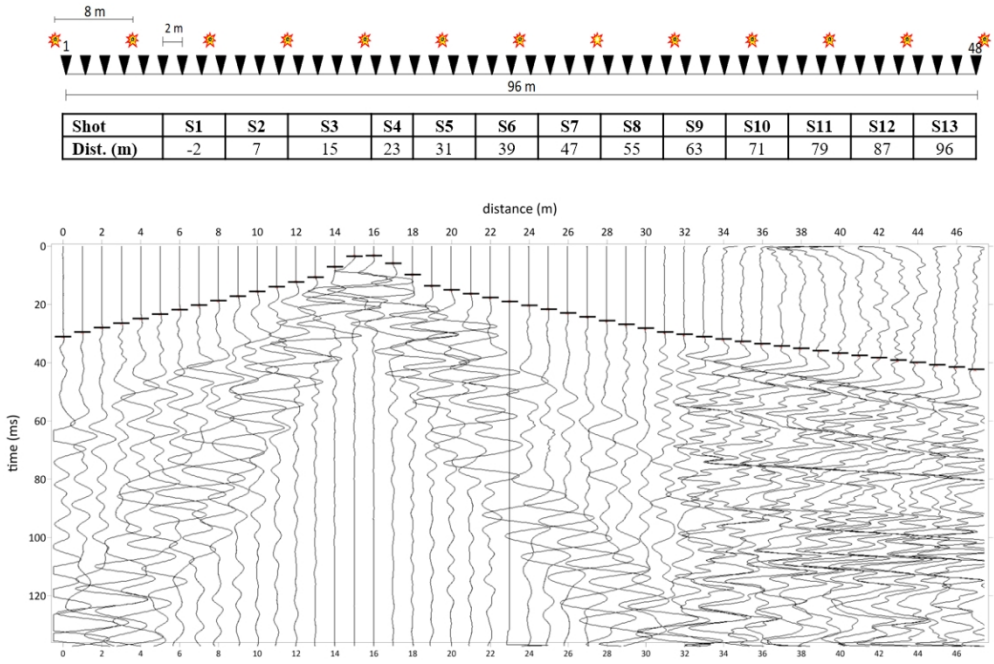

Shot	S1	S2	S3	S4	S5	S6	S7	S8	S9	S10	S11	S12	S13
Dist. (m)	-2	7	15	23	31	39	47	55	63	71	79	87	96

FIGURE 4: Surveying scheme of the Seismic Refraction Tomographies (top) and an example of seismograms related to the shot 5 of the SRTA (bottom), showing the picking of the first arrival times.

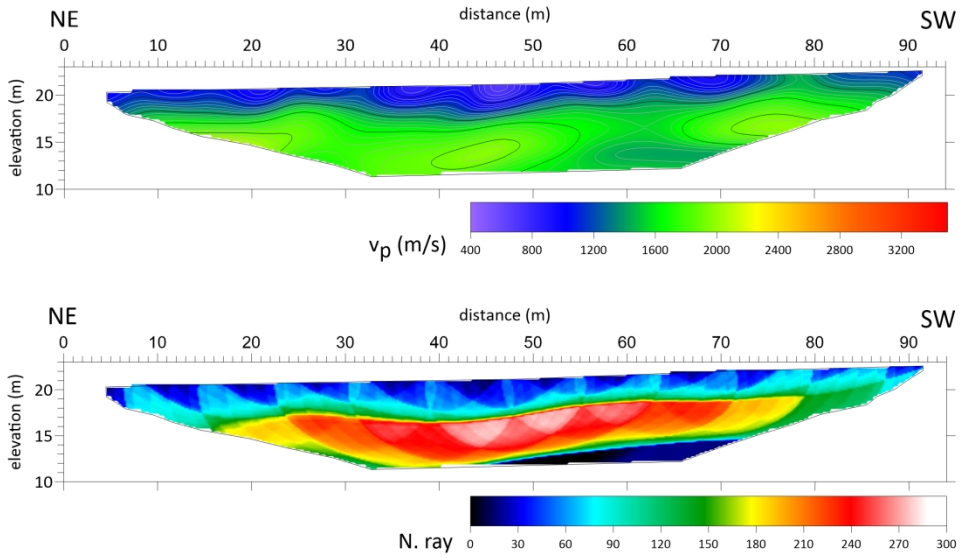

FIGURE 5: Seismic Refraction Tomography line A: P-waves velocity (top) and raypath density (bottom).

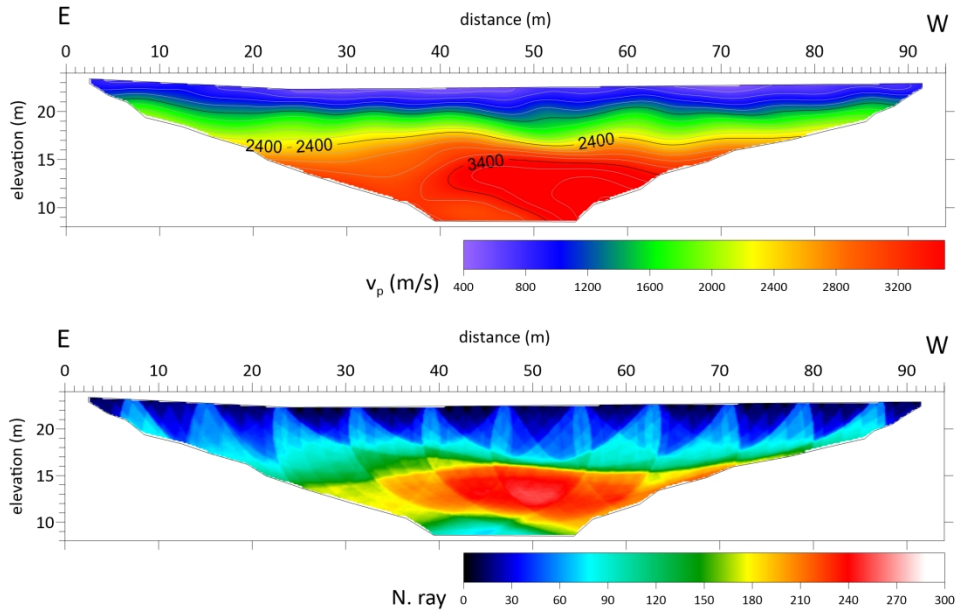

FIGURE 6: Seismic Refraction Tomography line B: P-waves velocity (top) and raypath density (bottom).

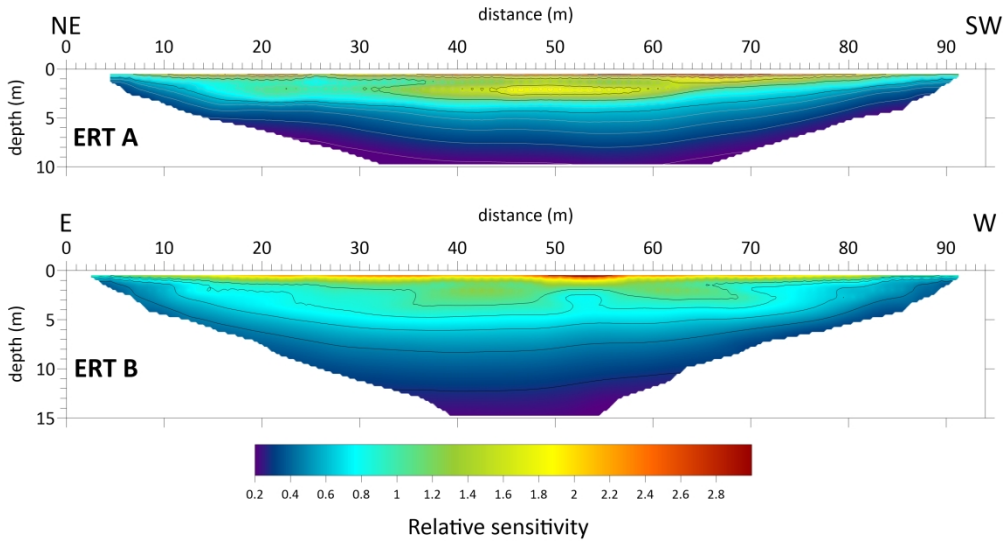

FIGURE 7: Pattern of the relative sensitivity of the electrical resistivity tomographies carried out in the Maredolce Lake.

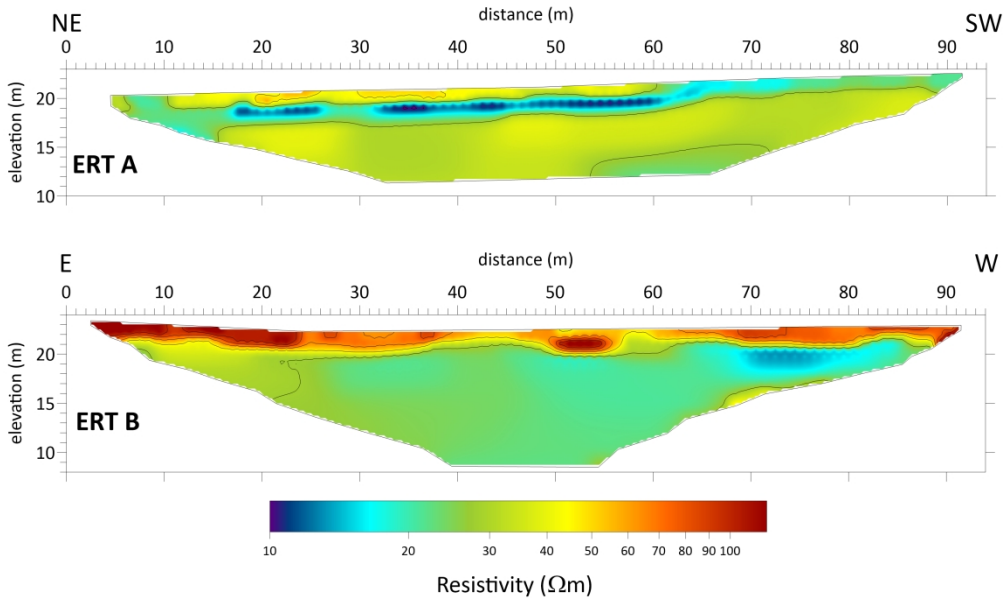

FIGURE 8: Electrical Resistivity Tomographies in the Maredolce Lake.

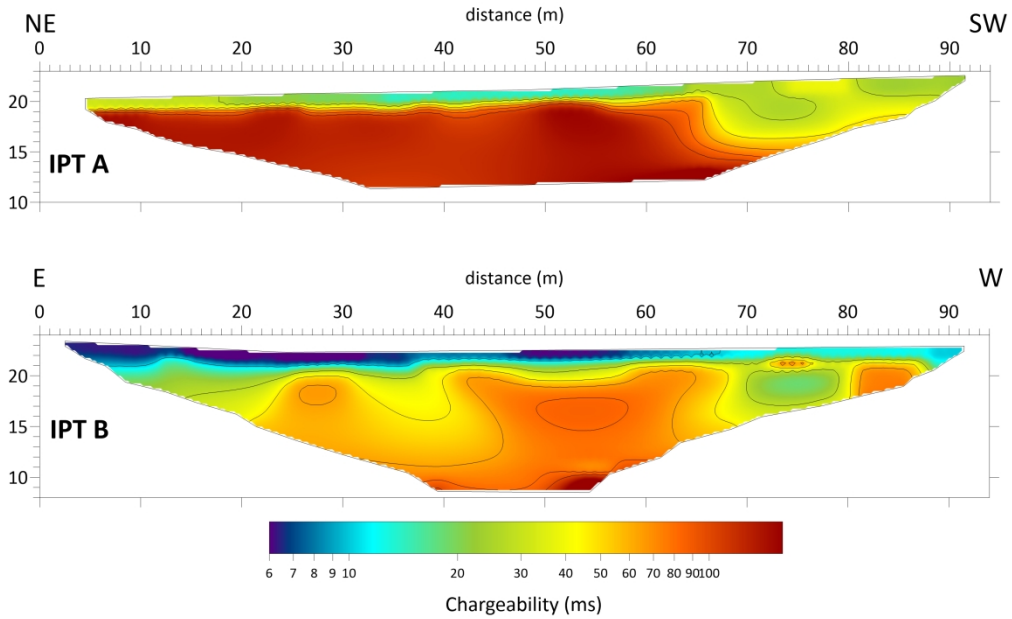

FIGURE 9: Induced Polarization Tomographies in the Maredolce Lake.

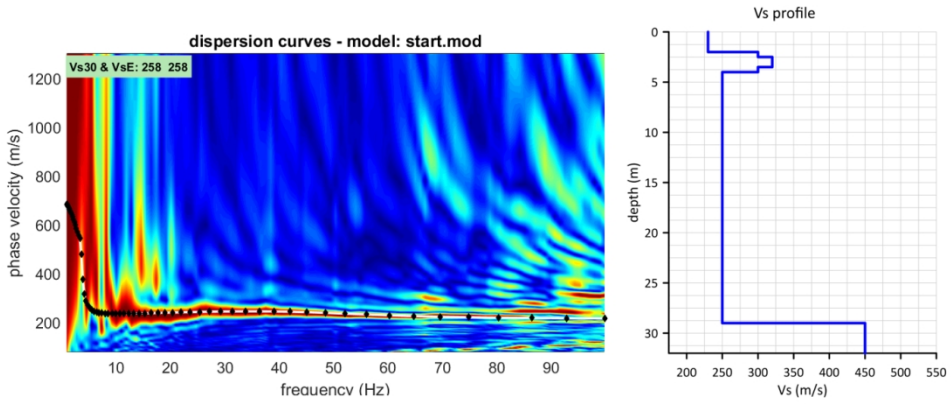

FIGURE 10: Results of the MASW1 analysis realized at the end of tomography line A. Dispersion curve picking in the frequency-phase velocity domain (on the left) and Vs vertical profile obtained from the analysis (on the right).

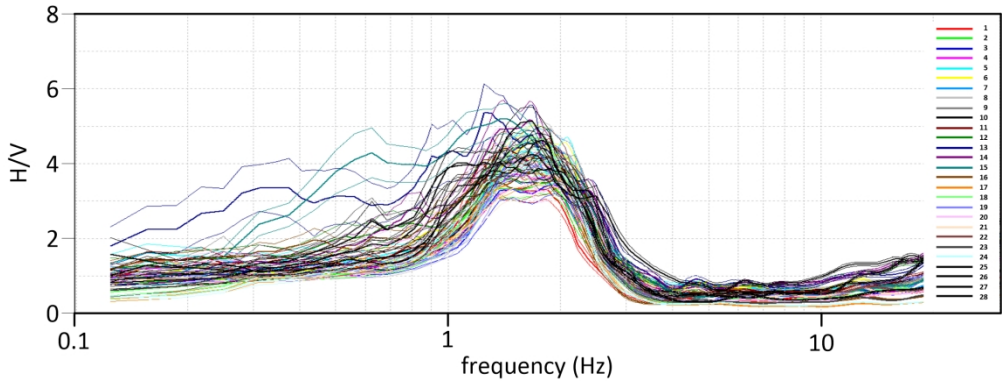

FIGURE 11: Representation of the HVSR curves obtained from the 28 microtremors acquisitions in Maredolce site.

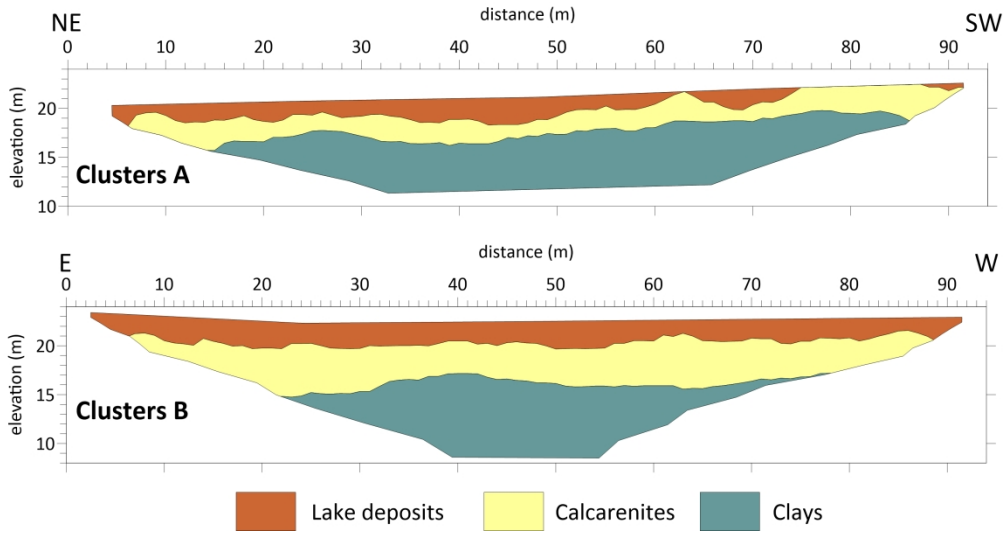

FIGURE 12: Results of the cluster analysis applied to ERT A and SRT A (top) and to ERT B and SRT B (bottom).

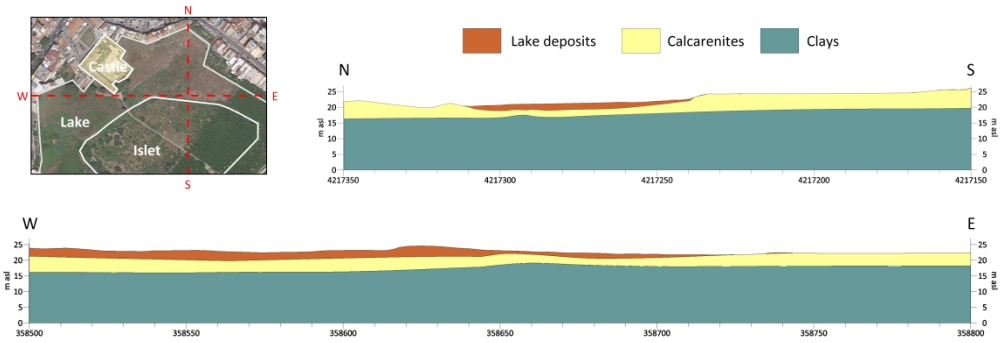

FIGURE 13: Vertical sections with directions N-S (top) and E-W (bottom) obtained from the 3D-stratigraphical model of the subsoil of the Maredolce Lake.

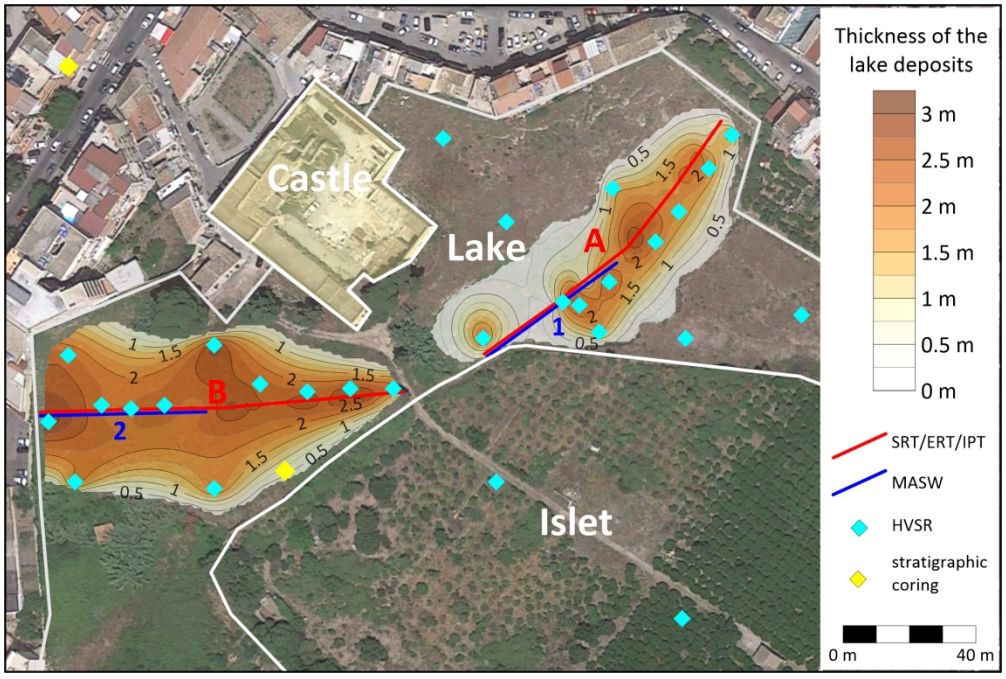

FIGURE 14: Isopach map of the lake deposits in the subsoil of the Maredolce Lake.

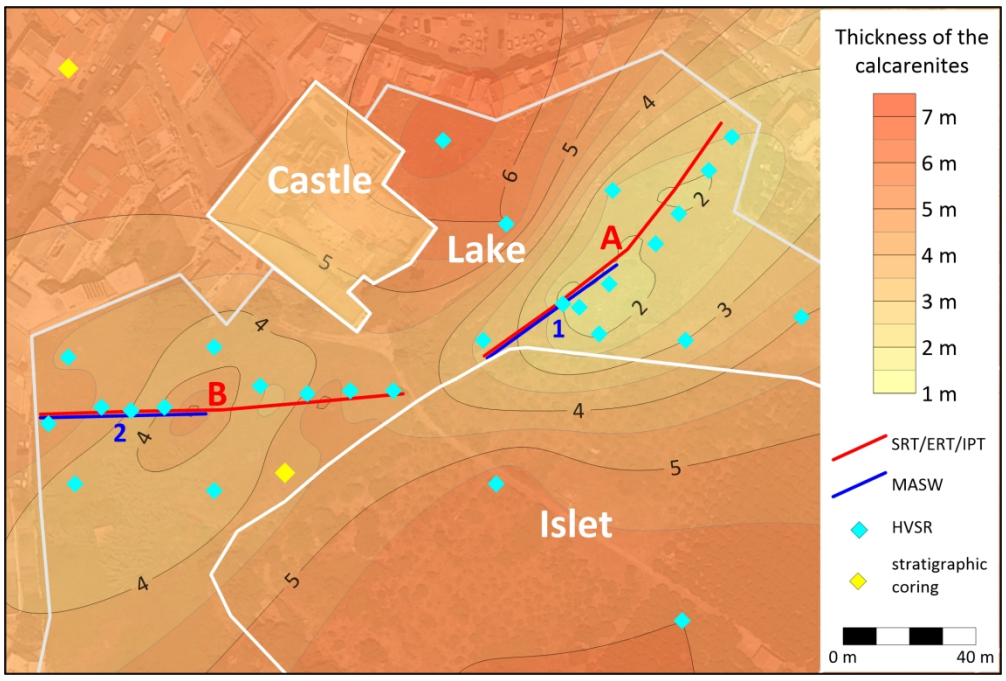

FIGURE 15: Isopach map of the Palermo calcarenites in the subsoil of the Maredolce Lake.

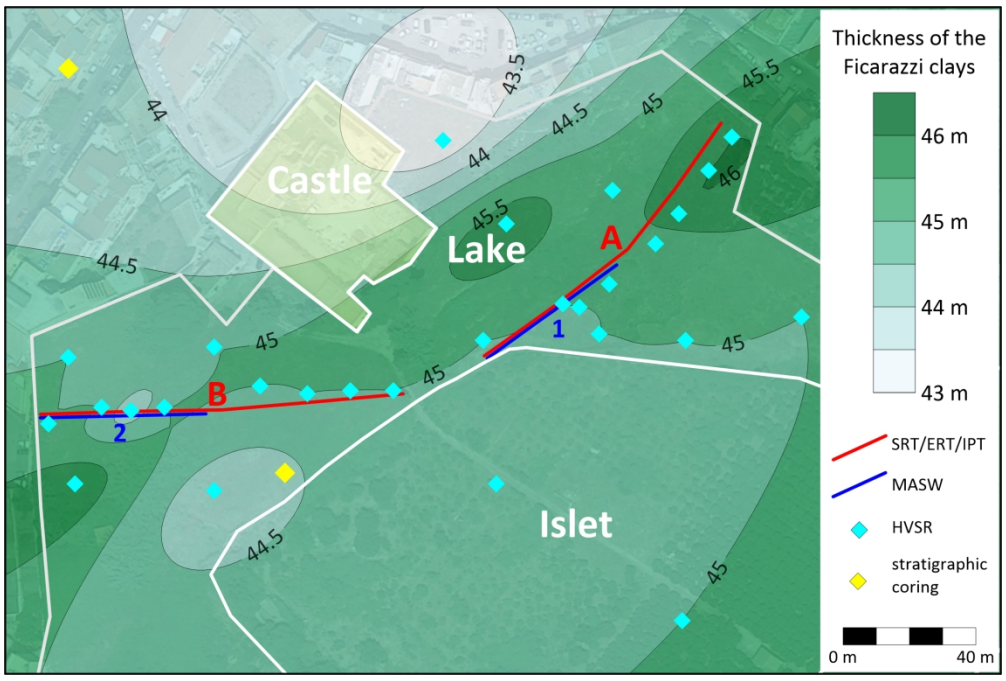

FIGURE 16: Isopach map of the Ficarazzi Clays in the subsoil of the Maredolce Lake.

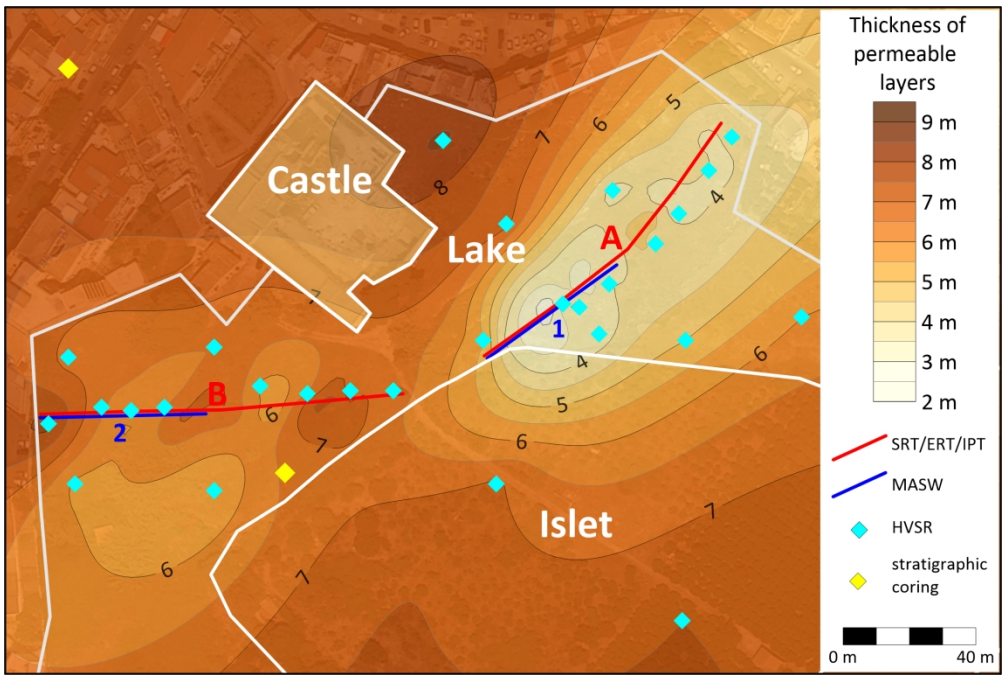

FIGURE 17: Isopach map of the permeable layers in the subsoil of the Maredolce Lake.